[3] U. Kuhl, M. Pauschinger, P.L. Schwimmbeck, B. Seeberg, C. Lober, M. Noutsias, M. Poller, H.P. Schultheiss, Interferon-beta treatment eliminates cardiotropic viruses and improves left ventricular function in patients with myocardial persistence of viral genomes and left ventricular dysfunction, Circulation 107 (2003) 2793–2798.

[4] D.M. McNamara, R. Holubkov, R.C. Starling, G.W. Dec, E. Loh, G. Torre-Amione, A. Gass, K. Janosko, T. Tokarczyk, P. Kessler, D.L. Mann, A.M. Feldman, Controlled trial of intravenous immune globulin in recent-onset dilated cardiomyopathy, Circulation 103 (2001) 2254–2259.

[5] T. Sudoh, N. Minamino, K. Kangawa, H. Matsuo, C-type natriuretic peptide (CNP): a new member of natriuretic peptide family identified in porcine brain, Biochem. Biophys. Res. Commun. 168 (1990) 863–870.

[6] M. Furuya, K. Aisaka, T. Miyazaki, N. Honbou, K. Kawashima, T. Ohno, S. Tanaka, N. Minamino, K. Kangawa, H. Matsuo, C-type natriuretic peptide inhibits intimal thickening after vascular injury, Biochem. Biophys. Res. Commun. 193 (1993) 248–253.

[7] T. Horio, T. Tokudome, T. Maki, F. Yoshihara, S. Suga, T. Nishikimi, M. Kojima, Y. Kawano, K. Kangawa, Gene expression, secretion, and autocrine action of C-type natriuretic peptide in cultured adult rat cardiac fibroblasts, Endocrinology 144 (2003) 2279–2284.

[8] T. Tokudome, T. Horio, T. Soeki, K. Mori, I. Kishimoto, S. Suga, F. Yoshihara, Y. Kawano, M. Kohno, K. Kangawa, Inhibitory effect of C-type natriuretic peptide (CNP) on cultured cardiac myocyte hypertrophy: interference between CNP and endothelin-1 signaling pathways, Endocrinology 145 (2004) 2131–2140.

[9] T. Soeki, I. Kishimoto, H. Okumura, T. Tokudome, T. Horio, K. Mori, K. Kangawa, C-type natriuretic peptide, a novel antifibrotic and antihypertrophic agent, prevents cardiac remodeling after myocardial infarction, J. Am. Coll. Cardiol. 45 (2005) 608–616.

[10] T. Kashimura, M. Hayashi, M. Kodama, M. Nakazawa, S. Abe, T. Yoshida, H. Tachikawa, H. Hanawa, K. Kato, K. Watanabe, Y. Aizawa, Effects of imidapril and TA-606 on rat dilated cardiomyopathy after myocarditis, Jpn. Heart J. 44 (2003) 735–744.

[11] M. Kodama, Y. Matsumoto, M. Fujiwara, F. Masani, T. Izumi, A. Shibata, A novel experimental model of giant cell myocarditis induced in rats by immunization with cardiac myosin fraction, Clin. Immunol. Immunopathol. 57 (1990) 250–262.

[12] D.J. Nunez, M.C. Dickson, M.J. Brown, Natriuretic peptide receptor mRNAs in the rat and human heart, J. Clin. Invest. 90 (1992) 1966–1971.

[13] M. Kodama, H. Hanawa, M. Saeki, H. Hosono, T. Inomata, K. Suzuki, A. Shibata, Rat dilated cardiomyopathy after autoimmune giant cell myocarditis, Circ. Res. 75 (1994) 278–284.

[14] T. Itoh, N. Nagaya, S. Murakami, T. Fujii, T. Iwase, H. Ishibashi-Ueda, C. Yutani, M. Yamagishi, H. Kimura, K. Kangawa, C-type natriuretic peptide ameliorates monocrotaline-induced pulmonary hypertension in rats, Am. J. Respir. Crit. Care Med. 170 (2004) 1204–1211.

[15] T. Igaki, H. Itoh, S.I. Suga, N. Hama, Y. Ogawa, Y. Komatsu, J. Yamashita, K. Doi, T.H. Chun, K. Nakao, Effects of intravenously administered C-type natriuretic peptide in humans: comparison with atrial natriuretic peptide, Hypertens. Res. 21 (1998) 7–13.

[16] A. Ahluwalia, R.J. MacAllister, A.J. Hobbs, Vascular actions of natriuretic peptides. Cyclic GMP-dependent and -independent mechanisms, Basic. Res. Cardiol. 99 (2004) 83–89.

[17] H. Osawa, H. Yamabe, M. Kaizuka, N. Tamura, S. Tsunoda, Y. Baba, K. Shirato, F. Tateyama, K. Okumura, C-type natriuretic peptide inhibits proliferation and monocyte chemoattractant protein-1 secretion in cultured human mesangial cells, Nephron 86 (2000) 467–472.

[18] S. Murakami, N. Nagaya, T. Itoh, T. Fujii, T. Iwase, K. Hamada, H. Kimura, K. Kangawa, C-type natriuretic peptide attenuates bleomycin-induced pulmonary fibrosis in mice, Am. J. Physiol. Lung Cell. Mol. Physiol. 287 (2004) L1172–L1177.

[19] K. Yamahara, H. Itoh, T.H. Chun, Y. Ogawa, J. Yamashita, N. Sawada, Y. Fukunaga, M. Sone, T. Yurugi-Kobayashi, K. Miyashita, H. Tsujimoto, H. Kook, R. Feil, D.L. Garbers, F. Hofmann, K. Nakao, Significance and therapeutic potential of the natriuretic peptides/cGMP/cGMP-dependent protein kinase pathway in vascular regeneration, Proc. Natl. Acad. Sci. USA 100 (2003) 3404–3409.

[20] R. Dong, P. Liu, L. Wee, J. Butany, M.J. Sole, Verapamil ameliorates the clinical and pathological course of murine myocarditis, J. Clin. Invest. 90 (1992) 2022–2030.

[21] J.C. Choy, A.H. Lui, F. Moien-Afshari, K. Wei, B. Yanagawa, B.M. McManus, I. Laher, Coxsackievirus B3 infection compromises endothelial-dependent vasodilation of coronary resistance arteries, J. Cardiovasc. Pharmacol. 43 (2004) 39–47.

STEM CELLS

STEM CELL GENETICS AND GENOMICS

Effect of Hypoxia on Gene Expression of Bone Marrow-Derived Mesenchymal Stem Cells and Mononuclear Cells

SHUNSUKE OHNISHI,[a] TAKESHI YASUDA,[b] SOICHIRO KITAMURA,[c] NORITOSHI NAGAYA[a]

Departments of [a]Regenerative Medicine and Tissue Engineering and [c]Cardiovascular Surgery, National Cardiovascular Center, Osaka, Japan; [b]GeneticLab Company, Ltd., Sapporo, Japan

Key Words. Microarray • Mononuclear cell • Mesenchymal stem cell • Hypoxia • Bone marrow

ABSTRACT

MSC have self-renewal and multilineage differentiation potential, including differentiation into endothelial cells and vascular smooth muscle cells. Although bone marrow-derived mononuclear cells (MNC) have been applied for therapeutic angiogenesis in ischemic tissue, little information is available regarding comparison of the molecular foundation between MNC and their MSC subpopulation, as well as their response to ischemic conditions. Thus, we investigated the gene expression profiles between MSC and MNC of rat bone marrow under normoxia and hypoxia using a microarray containing 31,099 genes. In normoxia, 2,232 (7.2%) and 2,193 genes (7.1%) were preferentially expressed more than threefold in MSC and MNC, respectively, and MSC expressed a number of genes involved in development, morphogenesis, cell adhesion, and proliferation, whereas various genes highly expressed in MNC were involved in inflammatory response and chemotaxis. Under hypoxia, 135 (0.44%) and 49 (0.16%) genes were upregulated (>threefold) in MSC and MNC, respectively, and a large number of those upregulated genes were involved in glycolysis and metabolism. Focusing on genes encoding secretory proteins, the upregulated genes in MSC under hypoxia included several molecules involved in cell proliferation and survival, such as vascular endothelial growth factor-D, placenta growth factor, pre-B-cell colony-enhancing factor 1, heparin-binding epidermal growth factor-like growth factor, and matrix metalloproteinase-9, whereas the upregulated genes in MNC under hypoxia included proinflammatory cytokines such as chemokine (C-X-C motif) ligand 2 and interleukin-1α. Our results may provide information on the differential molecular mechanisms regulating the properties of MSC and MNC under ischemic conditions. STEM CELLS *2007;25:1166–1177*

Disclosure of potential conflicts of interest is found at the end of this article.

INTRODUCTION

MSC possess multipotency and terminally differentiate into osteoblasts, chondrocytes, neurons, skeletal muscle cells, endothelial cells, and vascular smooth muscle cells [1, 2]. MSC can be easily isolated from bone marrow-derived mononuclear cells (MNC) and expanded in vitro >1 million-fold. Thus, these features make MSC an attractive therapeutic tool [1]. Although bone marrow-derived MNC have already been established as a tool for cell therapy and have been shown to induce therapeutic neovascularization in critical limb ischemia and myocardial infarction [3–6], MNC transplantation requires harvesting a large number of cells, and some patients are refractory to MNC therapy [7, 8]. We have previously demonstrated that MSC transplantation caused great improvement in rat hind limb ischemia and dilated cardiomyopathy [9, 10]. Recent studies suggest that MSC exert tissue regeneration through paracrine effects, as well as through differentiation into specific cell types [11, 12]. However, the molecular mechanisms that explain the difference between bone marrow-derived MNC and their MSC subpopulation exposed into ischemic conditions are yet to be studied. Thus, the purposes of this study were (a) to compare the gene expression profile of two fractions of clinically applicable bone marrow-derived cells (i.e., freshly isolated MNC versus their cultured MSC subpopulation), and (b) to investigate the effect of hypoxia on gene expression in MSC and MNC.

MATERIALS AND METHODS

Expansion of MSC and Isolation of MNC

Isolation and expansion of MSC were performed as described previously [13]. Briefly, bone marrow cells were isolated from male Lewis rats weighing 220–250 g by flushing out the femoral and tibial cavities with phosphate-buffered saline and plated onto 10-cm dishes in complete culture medium: α-minimal essential medium (Invitrogen, Carlsbad, CA, http://www.invitrogen.com), 10% fetal bovine serum (Invitrogen), 100 U/ml penicillin, and 100 μg/ml streptomycin (Invitrogen). Five days after plating, nonadherent cells were removed, and adherent cells were further propagated for 4–5 passages. These cells were previously demonstrated to be positive for CD29 and CD90 surface markers and negative for CD34 and CD45 [10]. MNC were isolated from whole bone marrow cells by density gradient centrifugation (Histopaque-1083; Sigma-Aldrich, St. Louis, http://www.sigmaaldrich.com). The Animal Care Committee of the National Cardiovascular Center approved the experimental protocol.

Correspondence: Noritoshi Nagaya, M.D., Ph.D., Department of Regenerative Medicine and Tissue Engineering, National Cardiovascular Center, 5-7-1 Fujishirodai, Osaka 565-8565, Japan. Telephone: 81-6-6833-5012; Fax: 81-6-6833-9865; e-mail: nnagaya@ri.ncvc.go.jp; or Shunsuke Ohnishi, M.D., Ph.D., Department of Regenerative Medicine and Tissue Engineering, National Cardiovascular Center, 5-7-1 Fujishirodai, Osaka 565-8565, Japan. Telephone: 81-6-6833-5012; Fax: 81-6-6833-9865; e-mail: sonishi@ri.ncvc.go.jp Received June 6, 2006; accepted for publication February 1, 2007; first published online in STEM CELLS *EXPRESS* February 8, 2007; available online without subscription through the open access option. 1066-5099/2007/$30.00/0 doi: 10.1634/stemcells.2006-0347

Table 1. Primer pairs designed for semiquantitative and quantitative reverse transcription-polymerase chain reaction

Target	Sense primer	Antisense primer
Semiquantitative		
AM	5′-gtggaataagtgggcgctaa-3′	5′-agggctgatcttgtttctgg-3′
COL3A1	5′-cgagattaaagcaagaggaa-3′	5′-gaggcttctttacataccac-3′
CXCL2	5′-tcctcaatgctgtactggtcc-3′	5′-atgttcttcctttccaggtc-3′
HB-EGF	5′-tcccactggaaccacaaaccag-3′	5′-cccacgatgacaagaagacagac-3′
IL-1α	5′-cgcttgagtcggcaaagaaatc-3′	5′-cacatgccatgcgagtgattag-3′
MIF	5′-caccatgcctatgttcatcgtgaaca-3′	5′-cggttccaccttcgcttgagcccggg-3′
MMP-9	5′-aaatgtgggtgtacacaggc-3′	5′-ttcacccggttgtggaaact-3′
MMP-14	5′-agtgccctatgcctacatcc-3′	5′-aatgggcattgggtatccgt-3′
PBEF1	5′-ttggttctggtggcgctttgctac-3′	5′-aaggtccctgctggtgtcctatgt-3′
PGF	5′-acagaaatggaagtggtg-3′	5′-ggctaataaatagagggtagg-3′
SERPINE1	5′-accctcagcatgttcattgc-3′	5′-ctcgttcacctcgatcttgac-3′
SERPINF1	5′-tcaccaaccctgacatccacag-3′	5′-actgccccttgaagtaagccac-3′
SERPINH1	5′-gggcaggatatgccaaggag-3′	5′-gttggcagtgcagatcggaa-3′
VEGF-A	5′-actggaccctggctttactc-3′	5′-acgcactccagggcttcatc-3′
VEGF-D	5′-tccaaacagctctttgagatatcag-3′	5′-ctccaggacatggtgctttaca-3′
GAPDH	5′-tgaaggtcggtgtcaacggatttggc-3′	5′-catgtaggccatgaggtccaccac-3′
Quantitative		
AM	5′-cctttcagcagggtatcgg-3′	5′-cacttattccacttctttcg-3′
CXCL2	5′-gccaccaaccatcagggtac-3′	5′-ccaggtcagttagccttgcct-3′
HB-EGF	5′-ctgagatggcggttccttaca-3′	5′-aggcccagtcagggtagca-3′
IL-1α	5′-agtcactcgcatggcatgtg-3′	5′-atatgtcgggctggttccac-3′
MIF	5′-gaaccgcaactacagcaagct-3′	5′-tggctgcgttcatgtcgtaa-3′
MMP-9	5′-ggcctatttctgccatgacaaatac-3′	5′-ctgcaccgctgaagcaaaag-3′
PBEF1	5′-ttggttctggtggcgctttgctac-3′	5′-aaggtccctgctggtgtcctatgt-3′
PGF	5′-catggactttgaccactgc-3′	5′-caagagaatctggcttggc-3′
VEGF-A	5′-acgaaagcgcaagaaatccc-3′	5′-ttaactcaagctgcctcgcc-3′
VEGF-D	5′-acaagatgagaatccactgcctgg-3′	5′-ctccaggacatggtgctttacaga-3′
GAPDH	5′-gttcttcaatacgtcagacattcg-3′	5′-cattatcttgctgtcacaagagc-3′

Culture of MSC and MNC Under Hypoxia

MSC and MNC (3×10^6 cells) were plated on 10-cm dishes in complete culture medium and incubated under normoxia (21% O_2, 5% CO_2) or hypoxia (1% O_2, 5% CO_2) for 24 hours. For time-dependent hypoxia experiments, cells were incubated for the desired time at 1% O_2. For the experiments with various O_2 levels, cells were incubated under the desired level of O_2 (1%, 3%, 10%, and 20%) for 24 hours.

Microarray Analysis

Total RNA was extracted from cells using an RNeasy Mini Kit (Qiagen, Hilden, Germany, http://www1.qiagen.com) according to the manufacturer's instructions. RNA was quantified by spectrometry, and the quality was confirmed by gel electrophoresis. Double-stranded cDNA was synthesized from 10 μg of total RNA, and in vitro transcription was performed to produce biotin-labeled cRNA using GeneChip One-Cycle Target Labeling and Control Reagents (Affymetrix, Santa Clara, CA, http://www.affymetrix.com) according to the manufacturer's instructions. After fragmentation, 10 μg of cRNA was hybridized with GeneChip Rat Genome 230 2.0 Array (Affymetrix) containing 31,099 genes. GeneChips were then scanned in a GeneChip Scanner 3000 (Affymetrix). Normalization, filtering, and Gene Ontology analysis of the data were performed with GeneSpring GX 7.3.1 software (Agilent Technologies, Palo Alto, CA, http://www.agilent.com). The raw data from each array were normalized as follows: each CEL file was preprocessed with robust multichip average, and each measurement for each gene was divided by the 50th percentile of all measurements. Genes with a change of at least threefold were then selected.

Semiquantitative Reverse Transcription-Polymerase Chain Reaction

Total RNA was extracted from separately prepared cells as described above, and 5 μg of total RNA was reverse-transcribed into cDNA using avian myeloblastosis virus transcriptase (Ambion, Austin, TX, http://www.ambion.com) and oligo(dT) primers. Polymerase chain reaction (PCR) amplification was performed in 50 μl containing 1 μl of cDNA and 2.5 U of Taq DNA polymerase (Takara, Otsu, Japan, http://www.takara.co.jp). The oligonucleotides used in semiquantitative reverse transcription (RT)-PCR analysis are listed in Table 1. Glyceraldehyde-3-phosphate dehydrogenase (GAPDH) mRNA amplified from the same samples served as an internal control. PCR mixtures were denatured at 95°C for 5 minutes, and cDNA templates were amplified as follows: 25 cycles (21 cycles for GAPDH) of denaturation at 95°C for 1 minute, annealing at 45–55°C for 45 seconds, and extension at 72°C for 1 minute. At the end of the cycling, the samples were incubated at 72°C for 10 minutes. The amplified DNA products were visualized on 2% agarose gels and photographed under ultraviolet light.

Quantitative Real-Time RT-PCR

PCR amplification was performed in 50 μl containing 1 μl of cDNA and 25 μl of Power SYBR Green PCR Master Mix (Applied BioSystems, Foster City, CA, http://www.appliedbiosystems.com). The oligonucleotides used in quantitative real-time RT-PCR analysis are listed in Table 1. GAPDH mRNA amplified from the same samples served as an internal control. After an initial denaturation at 95°C for 10 minutes, a 2-step cycle procedure was used (denaturation at 95°C for 15 seconds, annealing and extension at 60°C for 1 minute) for 40 cycles in a 7700 sequence detector (Applied Biosystems). Gene expression levels were normalized according to that of GAPDH and compared with that at normoxia (20% O_2). The data were analyzed with Sequence Detection Systems software (Applied BioSystems).

RESULTS

Reproducibility of Microarray Experiments

Reproducibility in the microarray experiment was assessed by repeated experiments using separately prepared RNAs. The correlation coefficient between two microarray data sets obtained from repeated experiments was greater than 0.98 for all

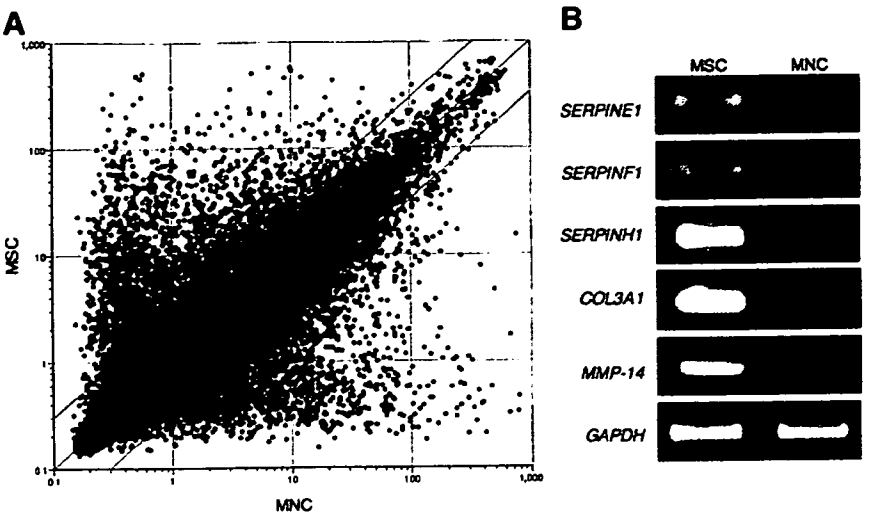

Figure 1. Expression profile of bone marrow-derived MSC versus MNC. (A): Normalized microarray data sets of MSC and MNC. All 31,099 gene probes are represented in this plot. The outer lines indicate a threefold difference, whereas the central line represents equality. (B): Semiquantitative reverse transcription-polymerase chain reaction of selected genes from Table 2, including serine protease inhibitors. GAPDH was used as an internal control. Abbreviations: GAPDH, glyceraldehyde-3-phosphate dehydrogenase; MNC, mononuclear cell.

gene probes, indicating that the whole experimental procedure was highly reproducible (data not shown).

Differentially Expressed Genes in Bone Marrow-Derived MSC and MNC Under Normoxia

Of 31,099 genes analyzed, 2,232 genes (7.2%) were highly expressed (>threefold) in MSC (Fig. 1A) and 55 genes (0.18%) were highly expressed more than 100-fold (Table 2), whereas 2,193 genes (7.1%) were highly expressed (>threefold) in MNC, and 69 genes (0.22%) were highly expressed more than 100-fold (Table 3). Noteworthy, the highly expressed genes in MSC (>threefold) included various types of molecules involved in biogenesis of extracellular matrix, such as collagens (Iα1, Iα2, IIIα1, IVα1, IVα2, Vα1, Vα2, VIα2, VIα3, VIIIα1, VIIIα2, XIα1, XIIα1, XIVα1, XV, XVIα1, and XVIIIα1), matrix metalloproteinases (MMP-2, -12, -14, -16, -19, and -23), serine proteases (PRSS9, 11, 23, and 35), and serine protease inhibitors (SERPINE1, SERPINF1, and SERPINH1). To verify the gene expression profile determined by our microarray analysis, the expression levels of serine protease inhibitors (SERPINE1, SERPINF1, and SERPINH1), COL3A1, and MMP-14 were analyzed by semiquantitative RT-PCR, using total RNAs separately obtained from MSC and MNC (Fig. 1B). The results showed that the differential expression pattern was in good agreement with that from the microarray analysis.

Functional Classification of Highly Expressed Genes in MSC and MNC Under Normoxia

To evaluate the enriched genes in MSC, a total of 2,232 highly represented genes (>threefold) were classified by functional annotation using gene ontology terms (Table 4). Nineteen terms in the list had a p value of less than .0001, including development (e.g., transgelin, actin-γ1, and short stature homeobox-2), morphogenesis (e.g., bone morphological protein-2, transforming growth factor-β3, and fibrillin-2), cell adhesion (e.g., melanoma cell adhesion molecule, neural cell adhesion molecule-1, and cadherin-11), and cell proliferation (e.g., connective tissue growth factor, fibroblast growth factor-7, and platelet-derived growth factor-A). On the other hand, for MNC, there were 30 listed terms from 2,193 enriched genes with a p value of less than .0001, including hemopoiesis, inflammatory response, and chemotaxis (Table 4).

Differentially Upregulated Genes in Bone Marrow-Derived MSC and MNC in Response to Hypoxia

To investigate the difference in gene expression in response to hypoxia, microarray analysis was performed using total RNAs obtained from MSC and MNC incubated under hypoxia for 24 hours (Fig. 2A; Tables 5 and 6). The results demonstrated that 135 (0.44%) and 49 (0.16%) genes were upregulated (>threefold) in MSC and MNC under hypoxia, respectively (Fig. 2B), and a significant number of those upregulated genes were involved in glycolysis and metabolism, according to gene ontology classification (data not shown). However, focusing on genes encoding secretory proteins, the upregulated genes in MSC under hypoxia included several molecules involved in cell proliferation and survival, such as vascular endothelial growth factor-D (*VEGF-D*), placenta growth factor (*PGF*), pre-B-cell colony-enhancing factor 1 (*PBEF1*), heparin binding epidermal growth factor-like growth factor (*HB-EGF*), and matrix metalloproteinase-9 (*MMP-9*), whereas the upregulated genes in MNC included some proinflammatory cytokines, such as chemokine (C-X-C motif) ligand 2 (*CXCL2*) and interleukin-1α (*IL-1α*) (Fig. 2B). Pairwise comparison of those upregulated genes from both MSC and MNC revealed that only 29 genes overlapped (21.3% in MSC and 59.2% in MNC), including *VEGF-A*, adrenomedullin (*AM*), and macrophage migration inhibitory factor (*MIF*) (Fig. 2B). Semiquantitative RT-PCR for those upregulated genes encoding secretory proteins confirmed the consistency of microarray data (Fig. 2C). To follow the kinetics of those upregulated genes, cells were cultured under different time points at 1% O_2 or different grades of hypoxia, and quantitative real-time RT-PCR was performed. The results demonstrated that the time course and sustainability of gene expression were differently regulated (Fig. 2D). The expression of all genes except *AM* was gradually increased in MSC under hypoxia, whereas *AM* expression was peaked at 12 hours and slightly decreased at 24 hours. On the other hand, the expression of *MIF*, *VEGF-A*, and *AM* in MNC were peaked at 6 hours and was sustained up to 24 hours, whereas the expression of *IL-1α* and *CXCL2* was gradually increased. When cells were cultured at different O_2 levels for 24 hours, most of the genes except *VEGF-D* were upregulated even at 10% O_2 in MSC, whereas the expression of three (*MIF*, *IL-1α*, and *CXCL2*) in MNC was unaffected at 10% O_2 and reached a peak at 1% O_2 (Fig. 2E).

Table 2. Genes upregulated in MSC (>100-fold)

Gene name	GenBank accession no.	Fold change
Collagen, type III, α1 (*COL3A1*)	BI275716	979.7
Transgelin (*TAGLN*)	NM_031549	918.1
Lysyl oxidase (*LOX*)	NM_017061	910.5
Follistatin-like 1 (*FSTL1*)	BG665037	689.4
Steroid sensitive gene 1 (*SSG1*)	AI235465	563.7
Collagen, type V, α2 (*COL5A2*)	AI179399	557.3
Actin, γ2 (*ACTG2*)	NM_012893	486.8
Protease, serine, 23 (*PRSS23*)	AI177099	427.2
Strongly similar to NP_035737.1 tenascin C (*TNC*)	AI176034	394.1
Serine proteinase inhibitor, clade H, member 1 (*SERPINH1*)	BI285495	379.7
Protein kinase C, δ binding protein (*PRKCDBP*)	NM_134449	352.3
Syndecan 2 (*SDC2*)	BG668421	315.5
Caveolin (*CAV*)	BI285449	313.6
Heat shock protein 1 (*HSPB1*)	NM_031970	312.8
Lysyl oxidase-like 2 (predicted)	AI044651	307.4
FAT tumor suppressor (*Drosophila*) homolog (*FATH*)	NM_031819	295.2
Protease, serine, 11 (*PRSS11*)	NM_031721	284.7
Arginase 1 (*ARG1*)	NM_017134	243.0
Cysteine knot superfamily 1, BMP antagonist 1 (*CKTSF1B1*)	NM_019282	231.9
Serine proteinase inhibitor, clade F, member 1 (*SERPINF1*)	AI179984	228.4
Serine proteinase inhibitor, clade E, member 1 (*SERPINE1*)	NM_012620	218.5
Nidogen (*NID*)	AI235948	214.4
Matrix metalloproteinase 14 (*MMP14*)	X83537	211.7
Lumican (*LUM*)	NM_031050	205.8
Transforming growth factor, β3 (*TGFB3*)	NM_013174	193.5
Cadherin 11 (*CDH11*)	BI296340	189.0
Par-4 (*PAWR*)	U05989	181.0
Collagen, type XI, α1 (*COL11A1*)	BM389291	179.1
Peptidylprolyl isomerase C (*PPIC*)	BI291292	170.5
A disintegrin and metalloproteinase with thrombospondin motifs 1 (*ADAMTS1*)	NM_024400	165.8
Interleukin 1 receptor-like 1 (*IL1RL1*)	NM_013037	153.9
WNT1 inducible signaling pathway protein 2 (*WISP2*)	NM_031590	153.3
Glypican 1 (*GPC1*)	NM_030828	150.0
Gap junction membrane channel protein α1 (*GJA1*)	AI411352	138.0
Matrix metalloproteinase 2 (*MMP2*)	U65656	131.2
Caldesmon 1 (CALD1)	BI291848	128.2
Growth factor receptor bound protein 14 (*GRB14*)	NM_031623	128.1
Coagulation factor 3 (*F3*)	NM_013057	127.1
Four and a half LIM domains 1 (*FHL1*)	BI298356	126.9
Calponin 1 (*CNN1*)	NM_031747	124.2
Tissue inhibitor of metalloproteinase 1 (*TIMP1*)	NM_053819	119.9
Strongly similar to NP_035711.1 thrombospondin 2 (*TSP-2*)	BF408413	119.4
Secreted acidic cysteine rich glycoprotein (*SPARC*)	NM_012656	118.7
Plastin 3 (*PLS3*)	BG672591	117.7
Superoxide dismutase 3 (*SOD3*)	NM_012880	116.4
Arginine vasopressin receptor 1A (*AVPR1A*)	NM_053019	114.7
Melanoma antigen, family D, 1 (*MAGED1*)	NM_053409	114.2
Tight junction protein 1 (*TJP1*)	AW434048	113.2
Connective tissue growth factor (*CTGF*)	NM_022266	109.8
LIM domain only protein 7 (*LMO7*)	AI598833	107.6
Tumor necrosis factor receptor superfamily, member 12a (*TNFRSF12A*)	BI303379	104.2
Actin, α1 (*ACTA1*)	NM_019212	104.2
Heart fatty acid binding protein 3 (*FABP3*)	NM_024162	103.8
Transforming growth factor, β2 (*TGFB2*)	BF420705	103.5
Short stature homeobox 2 (*SHOX2*)	NM_013028	101.4

DISCUSSION

In this study, we focused on differential gene expression of freshly isolated MNC and their cultured MSC subpopulation and the effect of hypoxia on gene expression of those cells. We showed that (a) MSC preferentially expressed a large number of genes involved in development, morphogenesis, cell adhesion, and cell proliferation, whereas MNC expressed various genes involved in inflammatory response and chemotaxis, and (b) MSC and MNC responded to hypoxia mostly in a distinct manner; several genes involved in cell proliferation and survival were upregulated in MSC, whereas some proinflammatory cytokines were upregulated in MNC.

In normoxia, MSC highly expressed various types of molecules that are considered to be essential for development and morphogenesis. Notably, the enriched genes in MSC included a number of molecules involved in biogenesis of extracellular matrix, such as collagens, MMPs, serine proteases, and serine protease inhibitors. MNC, on the other hand, highly expressed a large number of molecules involved in inflammatory response and chemotaxis. This result is largely consistent with a recent

Table 3. Genes upregulated in MNC (>100-fold)

Gene name	GenBank accession no.	Fold change
Hemoglobin α2 chain (*HBA-A1*)	AI179404	2,303
S100 calcium binding protein A9 (*S100A9*)	NM_053587	2,007
Hemoglobin β chain complex (*HBB*)	BI287300	1,996
Defensin Rat NP-3 precursor (*NP3B*)	U16683	1,439
S100 calcium binding protein A8 (*S100A8*)	NM_053822	1,274
Defensin Rat NP-4 precursor (*NP4*)	U16684	974.3
Ficolin B (*FCNB*)	NM_053634	813.6
Similar to Igh-6 protein (*IGH-6*)	AA996557	774.4
Mast cell protease 8 (*MCPT8*)	NM_021598	698.4
Chemokine (C-X-C motif) receptor 4 (*CXCR4*)	AA945737	694.5
Robo-1 (*ROBO-1*)	NM_031537	603.6
Carbonic anhydrase I (predicted)	BM383006	508.5
Serine (or cysteine) proteinase inhibitor, clade B, member 10 (*SERPINB10*)	BF399855	476.6
Similar to Ig heavy chain V-III region VH26 precursor (*IGHA*)	AI412189	459.9
Pre-eosinophil-associated ribonuclease-2	AI177934	430.9
Mast cell protease 9 (*MCPT9*)	NM_019323	409.6
Napsin A aspartic peptidase (*NAPSA*)	NM_031670	371.8
CD74 antigen (*CD74*)	NM_013069	369.3
Immunoglobulin joining chain (predicted)	AA817898	356
Mast cell protease 10 (*MCPT10*)	X68657	354.5
Similar to Myb proto-oncogene protein (*C-MYB*)	AI234125	341.6
Carbonic anhydrase 2 (*CA2*)	NM_019291	340.6
CD69 antigen (*CD69*)	AI137672	325.2
GDP dissociation inhibitor (*GDI*) β (predicted)	BF285771	321.8
Defensin, α5 (*DEFA*)	U16686	318.7
CD24 antigen (*CD24*)	BI285141	315.2
Transferrin (*TF*)	AA945178	269.8
CD37 antigen (*CD37*)	NM_017124	261.8
Cathepsin E (*CTSE*)	NM_012938	252.6
Coronin, actin binding protein 1A (*CORO1A*)	NM_130411	219.4
Lysosomal-associated protein transmembrane 5 (*LAPTM5*)	NM_053538	215.4
Macrophage expressed gene 1 (*MPEG1*)	AI170394	215.3
Protein tyrosine phosphatase, receptor type, C (*PTPRC*)	BF288130	207.5
Arginosuccinate synthetase (*AS*)	BF283456	205.1
Nuclear factor, erythroid derived 2 (predicted)	AW252129	198.2
Fibrinogen-like 2 (*FGL2*)	AI716194	197
Cytochrome b-245, β polypeptide (*CYBB*)	BE098739	196.7
Similar to RIKEN cDNA 1100001H23 (predicted)	BI285951	183.2
Leukocyte immunoglobulin-like receptor, subfamily B, member 3 (predicted)	AF169637	174
Matrix metallopeptidase 8 (*MMP8*)	NM_022221	173.6
CD53 antigen (*CD53*)	NM_012523	171.2
Complement component 3 (*C3*)	NM_016994	169.6
Aminolevulinic acid synthase 2 (*ALAS2*)	NM_013197	164.8
Similar to FCRL (predicted)	AI408164	163.4
Mast cell antigen 32 (*MCA32*)	NM_021585	161.2
Interleukin 1 receptor, type II (*IL1R2*)	NM_053953	161.2
Membrane-spanning 4-domains, subfamily A, member 1 (predicted)	AA817742	160.6
CD79B antigen (*CD79B*)	NM_133533	159.2
Homeobox only domain (*HOD*)	NM_133621	153.2
Chemokine (C-C motif) ligand 6 (*CCL6*)	BE095824	150.7
Similar to regulator of Fas-induced apoptosis	AI410062	148.3
RT1 class II, locus Bb (*RT1-BB*)	AI715202	146.2
Immunoglobulin superfamily, member 6 (*IGSF6*)	NM_133542	137.3
Pre-B lymphocyte gene 3 (predicted)	AW524266	130.9
Proteoglycan 2, bone marrow (*PRG2*)	NM_031619	126.5
Similar to GARP protein precursor (*GARPIN*) (predicted)	BM388665	125.4
Erythroid associated factor (predicted)	AI230287	124.6
Neurofibromatosis 1 (*NF1*)	BM386570	124
Similar to Rho GTPase activating protein 15	AI178168	123.1
RAS-related C3 botulinum substrate 2 (predicted)	AI010476	117.2
Natural killer cell group 7 sequence (*NKG7*)	NM_133540	113.2
Chemokine (C-X-C motif) ligand 2 (*CXCL2*)	NM_053647	112.3
Chymase 1, mast cell (*CMA1*)	NM_013092	108.8
Ras homolog gene family, member H (predicted)	AI012081	106.4
Similar to Clecsf12 protein	AI045955	105.8
Similar to protein tyrosine phosphatase 20	AW916153	105.1
Chemokine (C-C motif) receptor 2 (*CCR2*)	NM_021866	104.6
Solute carrier family 4, member 1 (*SLC4A1*)	BE113640	103.7
Thyroglobulin (*TG*)	AI500952	102.8

Abbreviation: MNC, mononuclear cells.

Table 4. Classification of highly expressed genes in MSC and MNC (>threefold) according to gene ontology terms

Category	% of genes in category	% of genes in list in category	p value
MSC			
0007275: development	23.2	35.8	1.1×10^{-12}
0007155: cell adhesion	5.7	12.7	5.1×10^{-11}
0048513: organ development	10.6	19.1	2.6×10^{-10}
0009653: morphogenesis	9.4	16.5	2.4×10^{-8}
0008283: cell proliferation	6.1	11.2	1.0×10^{-6}
0001501: skeletal development	2.1	5.3	1.2×10^{-6}
0016049: cell growth	1.8	4.8	1.3×10^{-6}
0009887: organ morphogenesis	5.0	9.5	2.3×10^{-6}
0008610: lipid biosynthesis	2.4	5.7	3.2×10^{-6}
0040007: growth	2.5	5.7	5.4×10^{-6}
0016125: sterol metabolism	1.1	3.3	6.8×10^{-6}
0009888: tissue development	2.6	5.9	7.2×10^{-6}
0016126: sterol biosynthesis	0.5	2.2	8.5×10^{-6}
0000074: regulation of progression through cell cycle	4.6	8.6	1.2×10^{-5}
0030324: lung development	0.6	2.2	1.3×10^{-5}
0007167: enzyme-linked receptor protein signaling pathway	3.1	6.4	1.4×10^{-5}
0000902: cellular morphogenesis	4.2	7.9	2.2×10^{-5}
0035295: tube development	0.9	2.9	2.4×10^{-5}
0001944: vasculature development	1.4	3.5	8.5×10^{-5}
MNC			
0009607: response to biotic stimulus	8.2	25.5	3.2×10^{-34}
0006952: defense response	8.0	24.9	2.4×10^{-33}
0006955: immune response	7.1	22.8	1.9×10^{-31}
0009611: response to wounding	4.7	12.6	4.3×10^{-13}
0009605: response to external stimulus	7.6	17.0	6.9×10^{-13}
0009613: response to pest, pathogen or parasite	4.6	11.9	2.8×10^{-12}
0006954: inflammatory response	2.5	7.3	3.3×10^{-9}
0001775: cell activation	1.6	5.4	5.4×10^{-9}
0006935: chemotaxis	1.5	5.0	3.1×10^{-8}
0006950: response to stress	10.7	18.6	4.0×10^{-8}
0048534: hemopoietic or lymphoid organ development	1.4	4.6	3.0×10^{-7}
0030097: hemopoiesis	1.4	4.6	3.0×10^{-7}
0030593: neutrophil chemotaxis	0.3	2.1	3.7×10^{-7}
0006968: cellular defense response	1.0	3.6	1.2×10^{-6}
0050874: organismal physiological process	23.0	32.0	1.2×10^{-6}
0050900: immune cell migration	0.5	2.5	1.3×10^{-6}
0006909: phagocytosis	0.4	2.1	1.5×10^{-6}
0030595: immune cell chemotaxis	0.5	2.3	2.6×10^{-6}
0050766: positive regulation of phagocytosis	0.2	1.5	4.6×10^{-6}
0046649: lymphocyte activation	1.3	4.0	5.4×10^{-6}
0001816: cytokine production	0.5	2.3	6.7×10^{-6}
0050778: positive regulation of immune response	0.6	2.5	7.7×10^{-6}
0030098: lymphocyte differentiation	0.6	2.5	1.1×10^{-5}
0042110: T-cell activation	0.9	2.9	2.5×10^{-5}
0045807: positive regulation of endocytosis	0.2	1.5	2.6×10^{-5}
0045576: mast cell activation	0.1	1.0	3.3×10^{-5}
0006911: phagocytosis, engulfment	0.1	1.0	3.3×10^{-5}
0030217: T-cell differentiation	0.4	1.9	6.5×10^{-5}
0001810: regulation of type I hypersensitivity	0.1	0.8	6.7×10^{-5}
0009617: response to bacteria	0.5	2.1	7.0×10^{-5}

Abbreviation: MNC, mononuclear cells.

report by Silva et al., which compared the gene expression of bone marrow-derived MSC with that of $CD34^+$ hematopoietic precursors by serial analysis of gene expression [14]. Recently, the differential gene expression profile of human umbilical cord blood (UCB)-derived MNC compared with their MSC subpopulation has been reported, and many of the genes listed as highly represented in UCB-derived MSC were identical to our results obtained from adult rat bone marrow [15]. Others have compared the gene expression profile of MSC with that of fibroblasts [16, 17]. However, there is no report regarding the gene expression profile of bone marrow-derived MSC, which are more relevant to clinical settings as a therapeutic tool than UCB-derived MSC, in comparison with bone marrow-derived MNC, which have already been applied for regenerative medicine [3–6]. Our results may provide information on the differential molecular mechanisms regulating the properties of bone marrow-derived MNC and their MSC subpopulation.

We have recently reported that MSC, in comparison with MNC, supplied larger amounts of angiogenic, antiapoptotic, and mitogenic factors such as VEGF, AM, hepatocyte growth factor and insulin-like growth factor-1, and some of the transplanted MSC survived even in an ischemic environment [9, 10]. Recent studies from other groups indicate that MSC mediate pleiotropic effects by secreting a large number of growth factors, antiapoptotic factors, and cytokines [11, 12, 18, 19]. Thus, it is of importance to investigate the difference in gene expression

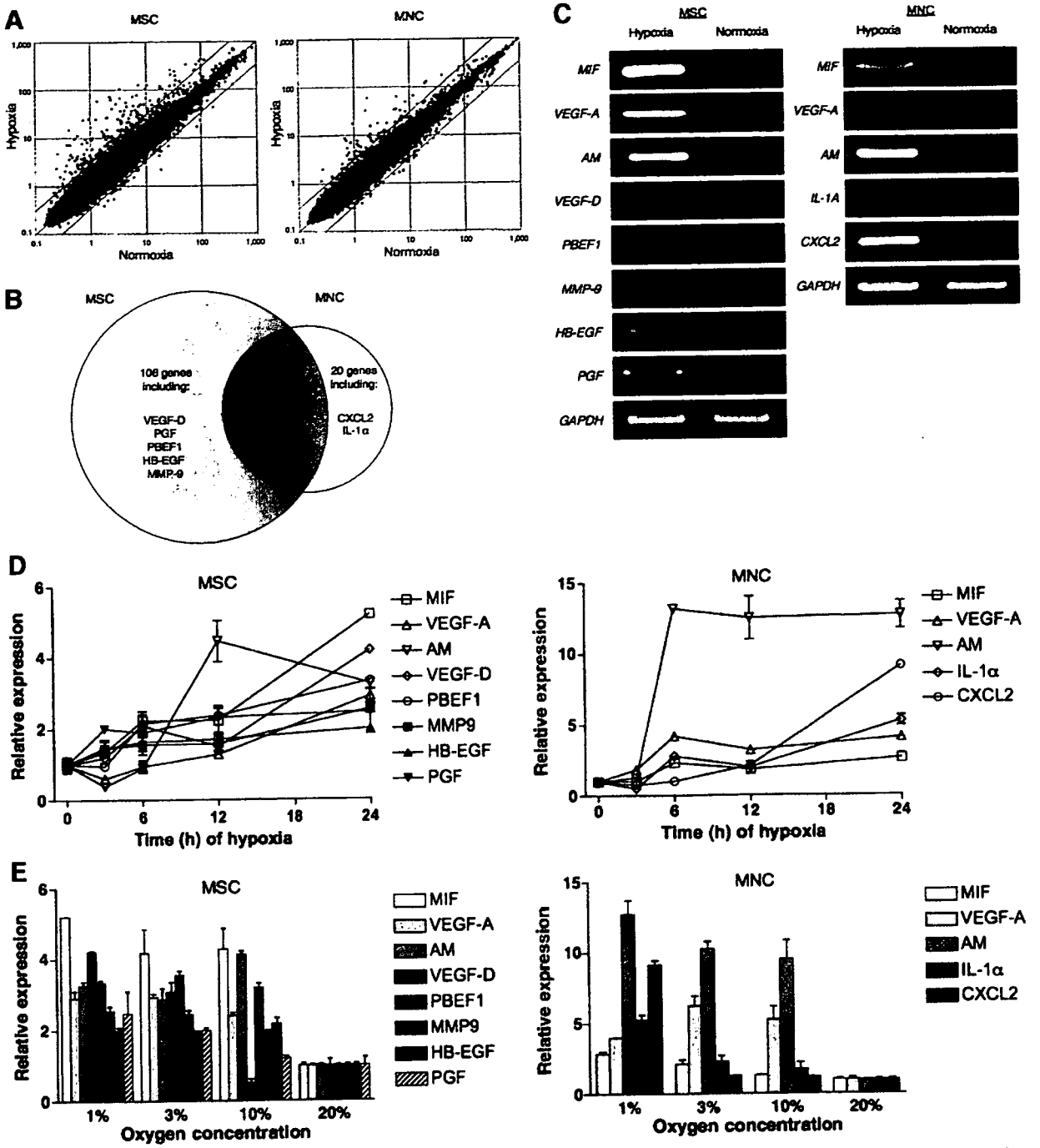

Figure 2. Expression profiles of MSC and MNC under normoxia versus hypoxia. **(A):** Normalized microarray data sets. All 31,099 gene probes are represented in this plot. The outer lines indicate a threefold difference, whereas the central line represents equality. **(B):** Pairwise comparison of upregulated genes from MSC and MNC under hypoxia. The numbers of genes upregulated more than threefold are presented. Gene symbols of selected secretory proteins are provided. **(C):** Semiquantitative reverse transcription-polymerase chain reaction (RT-PCR) of genes encoding secretory proteins listed in **(B)**. **(D):** Quantitative RT-PCR of genes encoding secretory proteins listed in **(B)** at different time points of 1% O_2. All transcription rates were estimated with reference to expression of each gene at normoxia (20% O_2). **(E):** Quantitative RT-PCR of genes encoding secretory proteins listed in **(B)** at different O_2 levels. All transcription rates were estimated with reference to expression of each gene at normoxia (20% O_2). Abbreviations: h, hours; MNC, mononuclear cell.

profile between MSC and MNC under hypoxia, which mimics the ischemic environment in vitro. Our observation revealed that MSC had more than five times as many exclusively upregulated genes as did MNC (106 vs. 20 genes), and only 29 genes, including *VEGF-A*, *AM*, and *MIF*, were commonly upregulated. This result is largely consistent with a very recent report by Martin-Rendon et al., which compared the gene expression of human cord blood $CD133^+$ cells with cultured bone marrow-derived MSC in response to hypoxia [20]. Although they cultured MNC in serum-free medium with cytokines such as IL-6, stem cell factor, Flt3-ligand, and thrombopoietin, the commonly upregulated genes in $CD133^+$ cells and MSC included *VEGF-A* and *AM*, in agreement with our results. MIF has been reported to be upregulated in response to hypoxia in glial tumor cells and

Table 5. Genes upregulated in MSC under hypoxia (>threefold)

Gene name	GenBank accession no.	Fold change
Cytochrome c oxidase, subunit 4b (*COX4B*)	NM_053472	33.2
Neuronal cell death inducible putative kinase (*NIPK*)	AB020967	33.0
ERO1-like (*ERO1L*)	AI146215	31.8
Solute carrier family 2, member 1 (*SLC2A1*)	BI284218	20.4
Serine hydroxymethyl transferase 2 (predicted)	BF411239	19.8
Liver glycogen phosphorylase (*PYGL*)	NM_022268	19.7
ATP-binding cassette, sub-family A (*ABC1*), member 4 (predicted)	AI602131	19.5
Putative ISG12(b) protein	AA819034	18.0
Enolase 2, γ (*ENO2*)	AF019973	17.5
Apelin (*APLN*)	AI177057	16.9
Metallothionein (*MT1A*)	AF411318	13.6
Hypoxia induced gene 1 (*HIG1*)	H31665	13.4
N-myc downstream regulated gene 1 (predicted)	BM384099	13.0
DNA-damage-inducible transcript 4 (*DDIT4*)	NM_080906	12.8
BCL2/adenovirus E1B 19 kDa-interacting protein 3 (*BNIP3*)	NM_053420	12.2
Adenylate kinase 3-like 1 (*AK3L1*)	AA891949	11.8
EGL nine homolog 1 (*EGLN1*)	BI282122	11.2
Similar to eukaryotic translation initiation factor 4E member 3	AI575608	11.0
Heme oxygenase 1 (*HMOX1*)	NM_012580	10.8
Caspase 11 (*CASP11*)	NM_053736	10.8
Similar to glutaminyl-peptide cyclotransferase precursor	BM390001	10.7
Adrenomedullin (*ADM*)	NM_012715	9.5
DNA-damage inducible transcript 3 (*DDIT3*)	NM_024134	9.3
N-myc downstream-regulated gene 2 (*NDRG2*)	NM_133583	9.1
Alcohol dehydrogenase 1 (*ADH1*)	NM_130780	8.8
Vascular endothelial growth factor A (*VEGFA*)	AF080594	8.2
Solute carrier family 16, member 3 (*SLC16A3*)	NM_030834	8.1
Aldolase C (*ALDOC*)	NM_012497	8.0
Stanniocalcin 1 (*STC1*)	BM386683	7.4
Macrophage migration inhibitory factor (*MIF*)	NM_031051	7.4
Phosphoglycerate kinase 1 (*PGK1*)	NM_053291	7.3
Similar to eukaryotic translation initiation factor 4E member 3	AI101338	7.0
Growth and transformation-dependent protein (*LOC60380*)	BE113639	6.8
Pyruvate dehydrogenase kinase 1 (*PDK1*)	NM_053826	6.7
Similar to von Willebrand factor A-domain-containing 1 (predicted)	BF413643	6.7
Procollagen-proline, 2-oxoglutarate 4-dioxygenase, α2 polypeptide (predicted)	BI274349	6.7
Procollagen-proline, 2-oxoglutarate 4-dioxygenase, α1 polypeptide (*P4HA1*)	BI274401	6.3
Asparagine synthetase (*ASNS*)	U07202	6.3
Hexokinase 2 (*HK2*)	BI294137	6.3
Strongly similar to NP_109603.2 glycogen synthase 1	BM392117	6.2
Glucan (1,4-α-), branching enzyme 1 (predicted)	BI284270	6.1
Activating transcription factor 5 (*ATF5*)	BM391471	6.0
Phosphofructokinase (*PFKL*)	NM_013190	5.8
Zinc finger protein 84 (predicted)	BI282114	5.7
Matrix metallopeptidase 9 (*MMP9*)	NM_031055	5.7
Triosephosphate isomerase 1 (*TPI1*)	NM_022922	5.6
CTL target antigen (*CTH*)	NM_017074	5.6
Glutamic pyruvate transaminase 2 (predicted)	AI454322	5.5
Phosphoserine aminotransferase 1 (*PSAT1*)	AI230228	5.4
Prostaglandin E synthase (*PTGES*)	AB048730	5.2
G protein-coupled receptor 128 (predicted)	BM388427	5.2
Rab40b, member RAS oncogene family (predicted)	AA924620	5.0
Inhibitor of DNA binding 2 (*ID2*)	AI008792	5.0
RAD23a homolog (predicted)	BF553981	5.0
Solute carrier family 2 (*SLC2A3*)	AA901341	4.9
Pre-B-cell colony enhancing factor 1 (*PBEF1*)	BI297612	4.8
Neural cell adhesion molecule 1 (*NCAM1*)	AI229409	4.7
Basic helix-loop-helix domain-containing, class B2 (*BHLHB2*)	NM_053328	4.7
Strongly similar to XP_579758.1 (predicted)	AI105202	4.7
Peptidoglycan recognition protein 1 (*PGLYRP1*)	NM_053373	4.6
Growth arrest specific 6 (*GAS6*)	H33111	4.6
Glucose phosphate isomerase (*GPI*)	BI283882	4.5
Cyclin G2 (predicted)	AI408309	4.5
O-Acyltransferase domain-containing 2 (predicted)	BG665934	4.5
Carbonic anhydrase 9 (predicted)	BM391835	4.4
Lactate dehydrogenase A (*LDHA*)	NM_017025	4.4
Similar to neuronal interacting factor X 1 (*NIX1*)	AI511126	4.4
Similar to phosphoglycerate mutase (EC 5.4.2.1) B chain	AI535383	4.4

Continued

Table 5. (continued)

Gene name	GenBank accession no.	Fold change
Phosphofructokinase, platelet (*PFKP*)	BM389769	4.3
Aldolase A (*ALDOA*)	NM_012495	4.3
Similar to synaptotagmin-like homologue lacking C2 domains-b	BF410325	4.2
Forkhead box K2 (predicted)	BF551356	4.1
Centaurin, β 1 (predicted)	BI275873	4.1
Max interacting protein 1 (*MXI1*)	AI409308	4.1
Protease, serine, 15 (*PRSS15*)	NM_133404	4.1
Phosphoenolpyruvate carboxykinase 2 (predicted)	AI228633	4.0
SNF1-like kinase (*SNF1LK*)	NM_021693	4.0
Formyltetrahydrofolate synthetase domain-containing 1 (predicted)	BF281848	4.0
Similar to cDNA sequence BC032204 (predicted)	AI045958	3.9
RAR-related orphan receptor α (predicted)	AI235414	3.9
Phosphoserine phosphatase (predicted) (*PSPH*)	BF282282	3.9
BM1k MHC class Ib antigen (*BM1*)	AJ243973	3.9
Rab26 (*RAB26*)	NM_133580	3.9
Cytochrome P450, family 26, subfamily b, polypeptide 1 (*CYP26B1*)	BF397093	3.9
Serine hydroxymethyl transferase 2 (*MGC105820*)	BF285150	3.8
3-phosphoglycerate dehydrogenase (*PHGDH*)	NM_031620	3.8
Tissue inhibitor of metalloproteinase 3 (*TIMP3*)	AI599265	3.8
Strongly similar to NP_076005.1 hypoxia-inducible protein 2	BI282296	3.8
Similar to B230212L03Rik protein	BG670960	3.8
Fatty acid binding protein 5, epidermal (*FABP5*)	U13253	3.7
Glutamyl-prolyl-tRNA synthetase (predicted)	AI234919	3.7
Very low density lipoprotein receptor (*VLDLR*)	AA849857	3.7
Eukaryotic translation initiation factor 4E binding protein 1 (*EIF4EBP1*)	NM_053857	3.7
Similar to RIKEN cDNA 2810428C21	BF407585	3.7
Keratin complex 2, basic, gene 8	BF281337	3.6
Enolase 1, α (*ENO1*)	NM_012554	3.6
Activating transcription factor 4 (*ATF4*)	NM_024403	3.6
Glutamic pyruvate transaminase (alanine aminotransferase) 2 (predicted)	AA955605	3.6
EGL nine homolog 3 (*EGLN3*)	NM_019371	3.6
LIM and senescent cell antigen-like domains 2 (predicted)	BI275904	3.6
Pre-mtHSP70	S75280	3.6
D site albumin promoter binding protein	AI230048	3.6
6-phosphofructo-2-kinase/fructose-2,6-biphosphatase 3 (*PFKFB3*)	D87247	3.5
Caspase 12 (*CASP12*)	NM_130422	3.5
A disintegrin-like and metalloprotease with thrombospondin type 1 motif, 8 (predicted)	AI577318	3.5
LOC362671 (predicted)	AI409584	3.4
Histone 2a (*H2A*)	BE104595	3.4
Phosphoglycerate mutase 1 (*PGAM1*)	NM_053290	3.4
Placental growth factor (*PGF*)	BF281271	3.4
CCAAT/enhancer binding protein, δ (*CEBPD*)	NM_013154	3.4
Activating transcription factor 3 (*ATF3*)	NM_012912	3.4
Heat shock protein, A (predicted)	BI282281	3.3
Pyruvate kinase, muscle (*PKM2*)	NM_053297	3.3
Histone 1, H2ai (predicted)	AI176481	3.3
Similar to RIKEN cDNA E130201N16 (predicted)	BE113624	3.2
Phosphoglucomutase 1 (*PGM1*)	NM_017033	3.2
Fos-like antigen 1 (*Fosl1*)	NM_012953	3.2
Growth arrest specific 5 (*GAS5*)	BF287008	3.2
Monoglyceride lipase (*MGLL*)	BG372713	3.2
Erythropoietin receptor (*EPOR*)	NM_017002	3.2
Solute carrier family 6, member 9 (*SLC6A9*)	M95413	3.2
Heparin-binding epidermal growth factor-like growth factor (*HB-EGF*)	NM_012945	3.1
Similar to genethonin 1 (predicted)	BI295979	3.1
Similar to 5830411E10Rik protein (predicted)	BI295501	3.1
Glutamate-cysteine ligase, catalytic subunit (*GCLC*)	AA892770	3.1
Neuronatin (*NNAT*)	NM_053601	3.1
Neurexophilin 4 (*NXPH4*)	NM_021680	3.1
Similar to hypothetical protein D4Ertd765e (predicted)	AI172274	3.1
Similar to RIKEN cDNA 4930455F23 (predicted)	BI281653	3.1
Zinc finger and BTB domain-containing 5 (predicted)	BI296566	3.0
Vascular endothelial growth factor-D (*VEGF-D*)	AY032728	3.0
Similar to SUMO/sentrin specific protease 5	BE110674	3.0
Mitogen activated protein kinase kinase 1 (*MAP2K1*)	D13341	3.0
Similar to RIKEN cDNA 0610007P06	AA891221	3.0
Protein phosphatase 1, regulatory subunit 3C (predicted)	AW530361	3.0

On the other hand, CXCL2 (macrophage inflammatory protein-2) and IL-1α were upregulated in MNC, but not in MSC, under hypoxia. Previous reports demonstrated that *CXCL2* gene expression is strongly induced in macrophages in response to hypoxia [40], and IL-1α production is also induced in peripheral blood MNC under hypoxia [41]. However, in contrast to MSC, no growth factors were specifically upregulated in MNC under hypoxia. It has been suggested that monocyte recruitment, as a consequence of an inflammatory response, is important for promoting angiogenesis via paracrine release of cytokines [42, 43]. Moreover, recent studies have suggested that transplantation of MNC, like that of MSC, induces therapeutic angiogenesis mostly through paracrine effects in ischemic disease [7, 44, 45]. Our observations suggest that transplantation of MNC, unlike that of MSC, may induce an inflammatory response under hypoxia, which may induce angiogenesis.

In the present study, we demonstrated that the gene responses to hypoxia at different time courses and different oxygen concentrations were cell-type-specific. In MSC, seven of the eight genes were upregulated even at 10% O_2 but responded slowly to hypoxia. On the contrary, three of the five enriched genes in MNC responded rapidly to hypoxia but did not reach a peak up to 1% O_2. It remains to be elucidated whether these differences contribute differently to paracrine actions of each type of cells in in vivo situations. Moreover, because bone marrow-derived MNC consists of mixed cell types, such as monocytes, lymphocytes, and erythroblasts, additional studies are needed to clarify which cell types in MNC are responsible for those gene expressions.

Taken together, the difference in gene expression profiles under normoxia and hypoxia, difference in gene expression at various times, and O_2 level between MSC and MNC could cause their distinctive paracrine effects in terms of cell proliferation, including angiogenesis, and cell survival.

SUMMARY

Bone marrow-derived MSC highly expressed a number of genes involved in development and morphogenesis compared with bone marrow-derived MNC. MSC and MNC responded to hypoxia mostly in an exclusive manner; this response might cause the difference in paracrine effects between MSC and MNC in ischemic conditions.

ACKNOWLEDGMENTS

This work was supported by a research Grant for Cardiovascular Disease (16C-6) and Human Genome Tissue Engineering 009 from the Ministry of Health, Labor and Welfare of Japan.

DISCLOSURE OF POTENTIAL CONFLICTS OF INTEREST

The authors indicate no potential conflicts of interest.

REFERENCES

1 Pittenger MF, Martin BJ. Mesenchymal stem cells and their potential as cardiac therapeutics. Circ Res 2004;95:9–20.
2 Minguell JJ, Erices A, Conget P. Mesenchymal stem cells. Exp Biol Med (Maywood) 2001;226:507–520.
3 Tateishi-Yuyama E, Matsubara H, Murohara T et al. Therapeutic angiogenesis for patients with limb ischaemia by autologous transplantation of bone-marrow cells: A pilot study and a randomised controlled trial. Lancet 2002;360:427–435.
4 Tse HF, Kwong YL, Chan JK et al. Angiogenesis in ischaemic myocardium by intramyocardial autologous bone marrow mononuclear cell implantation. Lancet 2003;361:47–49.
5 Perin EC, Dohmann HF, Borojevic R et al. Transendocardial, autologous bone marrow cell transplantation for severe, chronic ischemic heart failure. Circulation 2003;107:2294–2302.
6 Fernández-Aviles F, San Roman JA, Garcia-Frade J et al. Experimental and clinical regenerative capability of human bone marrow cells after myocardial infarction. Circ Res 2004;95:742–748.
7 Kinnaird T, Stabile E, Burnett MS et al. Bone-marrow-derived cells for enhancing collateral development: Mechanisms, animal data, and initial clinical experiences. Circ Res 2004;95:354–363.
8 Hattori R, Matsubara H. Therapeutic angiogenesis for severe ischemic heart diseases by autologous bone marrow cells transplantation. Mol Cell Biochem 2004;264:151–155.
9 Iwase T, Nagaya N, Fujii T et al. Comparison of angiogenic potency between mesenchymal stem cells and mononuclear cells in a rat model of hindlimb ischemia. Cardiovasc Res 2005;66:543–551.
10 Nagaya N, Kangawa K, Itoh T et al. Transplantation of mesenchymal stem cells improves cardiac function in a rat model of dilated cardiomyopathy. Circulation 2005;112:1128–1135.
11 Kinnaird T, Stabile E, Burnett MS et al. Local delivery of marrow-derived stromal cells augments collateral perfusion through paracrine mechanisms. Circulation 2004;109:1543–1549.
12 Kinnaird T, Stabile E, Burnett MS et al. Marrow-derived stromal cells express genes encoding a broad spectrum of arteriogenic cytokines and promote in vitro and in vivo arteriogenesis through paracrine mechanisms. Circ Res 2004;94:678–685.
13 Wakitani S, Saito T, Caplan AI. Myogenic cells derived from rat bone marrow mesenchymal stem cells exposed to 5-azacytidine. Muscle Nerve 1995;18:1417–1426.
14 Silva WA Jr, Covas DT, Panepucci RA et al. The profile of gene expression of human marrow mesenchymal stem cells. STEM CELLS 2003;21:661–669.
15 Jeong JA, Hong SH, Gang EJ et al. Differential gene expression profiling of human umbilical cord blood-derived mesenchymal stem cells by DNA microarray. STEM CELLS 2005;23:584–593.
16 Wagner W, Wein F, Seckinger A et al. Comparative characteristics of mesenchymal stem cells from human bone marrow, adipose tissue, and umbilical cord blood. Exp Hematol 2005;33:1402–1416.
17 Brendel C, Kuklick L, Hartmann O et al. Distinct gene expression profile of human mesenchymal stem cells in comparison to skin fibroblasts employing cDNA microarray analysis of 9600 genes. Gene Expr 2005; 12:245–257.
18 Gnecchi M, He H, Liang OD et al. Paracrine action accounts for marked protection of ischemic heart by Akt-modified mesenchymal stem cells. Nat Med 2005;11:367–368.
19 Gnecchi M, He H, Noiseux N et al. Evidence supporting paracrine hypothesis for Akt-modified mesenchymal stem cell-mediated cardiac protection and functional improvement. FASEB J 2006;20:661–669.
20 Martin-Rendon E, Hale SJ, Ryan D et al. Transcriptional profiling of human cord blood CD133+ and cultured bone marrow mesenchymal stem cells in response to hypoxia. STEM CELLS 2007;25:XX–XX.
21 Bacher M, Schrader J, Thompson N et al. Up-regulation of macrophage migration inhibitory factor gene and protein expression in glial tumor cells during hypoxic and hypoglycemic stress indicates a critical role for angiogenesis in glioblastoma multiforme. Am J Pathol 2003;162:11–17.
22 Baugh JA, Gantier M, Li L et al. Dual regulation of macrophage migration inhibitory factor (MIF) expression in hypoxia by CREB and HIF-1. Biochem Biophys Res Commun 2006;347:895–903.
23 Jussila L, Alitalo K. Vascular growth factors and lymphangiogenesis. Physiol Rev 2002;82:673–700.
24 Teng X, Li D, Johns RA. Hypoxia up-regulates mouse vascular endothelial growth factor D promoter activity in rat pulmonary microvascular smooth-muscle cells. Chest 2002;121(suppl 3):82S–83S.
25 Nilsson I, Rolny C, Wu Y et al. Vascular endothelial growth factor receptor-3 in hypoxia-induced vascular development. FASEB J 2004;18: 1507–1515.
26 Green CJ, Lichtlen P, Huynh NT et al. Placenta growth factor gene expression is induced by hypoxia in fibroblasts: A central role for metal transcription factor-1. Cancer Res 2001;61:2696–2703.
27 Samal B, Sun Y, Stearns G et al. Cloning and characterization of the cDNA encoding a novel human pre-B-cell colony-enhancing factor. Mol Cell Biol 1994;14:1431–1437.
28 Segawa K, Fukuhara A, Hosogai N et al. Visfatin in adipocytes is

upregulated by hypoxia through HIF1alpha-dependent mechanism. Biochem Biophys Res Commun 2006;349:875–882.
29 Bae SK, Kim SR, Kim JG et al. Hypoxic induction of human visfatin gene is directly mediated by hypoxia-inducible factor-1. FEBS Lett 2006;580:4105–4113.
30 Higashiyama S, Abraham JA, Miller J et al. A heparin-binding growth factor secreted by macrophage-like cells that is related to EGF. Science 1991;251:936–939.
31 Abramovitch R, Neeman M, Reich R et al. Intercellular communication between vascular smooth muscle and endothelial cells mediated by heparin-binding epidermal growth factor-like growth factor and vascular endothelial growth factor. FEBS Lett 1998;425:441–447.
32 Arkonac BM, Foster LC, Sibinga NE et al. Vascular endothelial growth factor induces heparin-binding epidermal growth factor-like growth factor in vascular endothelial cells. J Biol Chem 1998;273:4400–4405.
33 Krampera M, Pasini A, Rigo A et al. HB-EGF/HER-1 signaling in bone marrow mesenchymal stem cells: Inducing cell expansion and reversibly preventing multilineage differentiation. Blood 2005;106:59–66.
34 Jin K, Mao XO, Sun Y et al. Heparin-binding epidermal growth factor-like growth factor: Hypoxia-inducible expression in vitro and stimulation of neurogenesis in vitro and in vivo. J Neurosci 2002;22:5365–5373.
35 Chang C, Werb Z. The many faces of metalloproteases: Cell growth, invasion, angiogenesis and metastasis. Trends Cell Biol 2001;11:S37–43.
36 Vu TH, Shipley JM, Bergers G et al. MMP-9/gelatinase B is a key regulator of growth plate angiogenesis and apoptosis of hypertrophic chondrocytes. Cell 1998;93:411–422.
37 Johnson C, Sung HJ, Lessner SM et al. Matrix metalloproteinase-9 is required for adequate angiogenic revascularization of ischemic tissues: Potential role in capillary branching. Circ Res 2004;94:262–268.
38 Heissig B, Hattori K, Dias S et al. Recruitment of stem and progenitor cells from the bone marrow niche requires MMP-9 mediated release of kit-ligand. Cell 2002;109:625–637.
39 Jin DK, Shido K, Kopp HG et al. Cytokine-mediated deployment of SDF-1 induces revascularization through recruitment of CXCR4(+) hemangiocytes. Nat Med 2006;12:557–567.
40 Zampetaki A, Mitsialis SA, Pfeilschifter J et al. Hypoxia induces macrophage inflammatory protein-2 (MIP-2) gene expression in murine macrophages via NF-kappaB: The prominent role of p42/ p44 and PI3 kinase pathways. FASEB J 2004;18:1090–1092.
41 Ghezzi P, Dinarello CA, Bianchi M et al. Hypoxia increases production of interleukin-1 and tumor necrosis factor by human mononuclear cells. Cytokine 1991;3:189–194.
42 Arras M, Ito WD, Scholz D et al. Monocyte activation in angiogenesis and collateral growth in the rabbit hindlimb. J Clin Invest 1998;101:40–50.
43 Sunderkötter C, Steinbrink K, Goebeler M et al. Macrophages and angiogenesis. J Leukoc Biol 1994;55:410–422.
44 Balsam LB, Wagers AJ, Christensen JL et al. Haematopoietic stem cells adopt mature haematopoietic fates in ischaemic myocardium. Nature 2004;428:668–673.
45 Murry CE, Soonpaa MH, Reinecke H et al. Haematopoietic stem cells do not transdifferentiate into cardiac myocytes in myocardial infarcts. Nature 2004;428:664–668.

Circ J 2007; **Suppl A:** A-32–A-39

Mechanism and New Findings in Brugada Syndrome

Wataru Shimizu, MD; Takeshi Aiba, MD; Shiro Kamakura, MD

Brugada syndrome is a clinical entity characterized by coved type ST-segment elevation in the right precordial electrocardiographic leads (V_{1-3}) and an episode of ventricular fibrillation in the absence of structural heart disease. Although a number of clinical and experimental reports have elucidated the electrocardiographic, electrophysiologic, cellular, and molecular aspects, several problems remain unsolved. Recently developed high-resolution optical mapping techniques in arterially-perfused wedge preparations enable recording of transmembrane action potentials from 256 sites simultaneously at the epicardial surface, thus providing further advances in the understanding of the cellular mechanism of the specific ST-segment elevation and subsequent ventricular arrhythmias. In this review article, new findings relating to several unresolved problems such as gender difference (male predominance) and ethnic difference (higher incidence in Asian population) are also presented. (*Circ J* 2007; **Suppl A:** A-32–A-39)

Key Words: Brugada syndrome; Ethnicity; Gender; Genetics; Mutation; Polymorphism; ST-segment; Ventricular fibrillation

Brugada syndrome (BS) is characterized by coved-type ST-segment elevation in the right precordial electrocardiography (ECG) leads (V_{1-3}) and an episode of ventricular fibrillation (VF) in the absence of acute ischemia, electrolyte abnormalities or structural heart disease![1–8] A type-1 ST-segment elevation, which is defined as a coved ST-segment elevation of ≥0.2 mV at the J point with or without a terminal negative T wave, is required to diagnose BS, regardless of the absence or presence of sodium-channel blockers (Figs 1A,B)[7] A type-1 ST-segment elevation recorded only in the higher V_{1-2} leads (ie, 3rd and 2nd intercostal spaces) has been suggested to show similar prognostic value for subsequent cardiac events as that recorded in the standard V_{1-2} leads (Fig 1C)[7,9,10] A type-2 saddle-back ST-segment elevation alone is not diagnostic for BS (Fig 1B). The prevalence of this syndrome is estimated to be 5 per 10,000 inhabitants, and is one of the important causes of sudden cardiac death of middle-aged males in Asian countries particularly![11,12] BS usually manifests during adulthood, with a mean age of sudden death of 41±15 years, and child cases are rare[7] A family history of unexplained sudden death is present in approximately 20–40% of the population in Western countries, and less (15–20%) in Japan[4,7,13,14] A significant male predominance in BS has long been reported, and more than 80% of patients in Western countries and more than 90% of patients in Asian countries affected with BS are men![5] Since Brugada and Brugada described 8 patients with a history of aborted sudden cardiac death caused by VF as a distinct clinical entity in 1992[1] a number of clinical and experimental reports from around the world have demonstrated the clinical, electrocardiographic, electrophysiologic, cellular, ionic, genetic and molecular features of BS[2–14] However, several problems remain unsolved, such as genetic heterogeneity, late onset of first cardiac events, and gender and ethnic differences[8] In this review article, we present our recent data relating to the cellular and molecular mechanism of BS, the late onset of its clinical manifestation, male predominance, and higher incidence in Asian populations.

(Received January 25, 2007; revised manuscript received February 7, 2007; accepted February 8, 2007)

Division of Cardiology, Department of Internal Medicine, National Cardiovascular Center, Suita, Japan

Mailing address: Wataru Shimizu, MD, Division of Cardiology, Department of Internal Medicine, National Cardiovascular Center, 5-7-1 Fujishiro-dai, Suita 565-8565 Japan. E-mail: wshimizu@hsp.ncvc.go.jp

Genetic and Molecular Aspects

Advances in molecular genetics in the past decade have established a link between several inherited cardiac arrhythmias, including BS and long QT syndrome, and mutations in genes encoding ion channels, membrane components or receptors![16] In 1998, the first mutation linked to BS was identified by Chen et al in *SCN5A*![17] the gene encoding the α subunit of the sodium channel. Thereafter, a large family of BS was reported to link to a second locus on chromosome 3, which is close to but different from the *SCN5A* locus;[18] however, specific gene or genes other than *SCN5A* have not yet been identified on chromosome 3. *SCN5A* mutations are reported to account for 18–30% of clinically diagnosed BS patients at present[7] Antzelevitch et al have recently reported that 3 probands associated with a BS-like ST-segment elevation and a short QT interval were linked to mutations in *CACNA1C* (A39V and G490R) or *CACNB2* (S481L), the gene encoding the α1 or β2b subunit of the L-type calcium channel, respectively![19] Their genetic and heterologous expression studies revealed loss of function of the L-type calcium channel current ($I_{Ca\text{-}L}$). However, approximately two-thirds of BS patients have not been yet genotyped, suggesting the presence of genetic heterogeneity[8] Other candidate genes for the Brugada phenotype include those encoding the transient outward current (I_{to}) and the delayed rectifier potassium current (I_K), or those coding the adrenergic receptors, cholinergic receptors, ion-channel-interacting protein, promoters, transcriptional factors, neurotransmitters, or transporters[7,8]

Among the approximately 100 mutations in *SCN5A* linked to BS, some of them have been studied in expression systems, and have been shown to result in loss of function of the sodium channel current (I_{Na}) by several mechanisms[20]

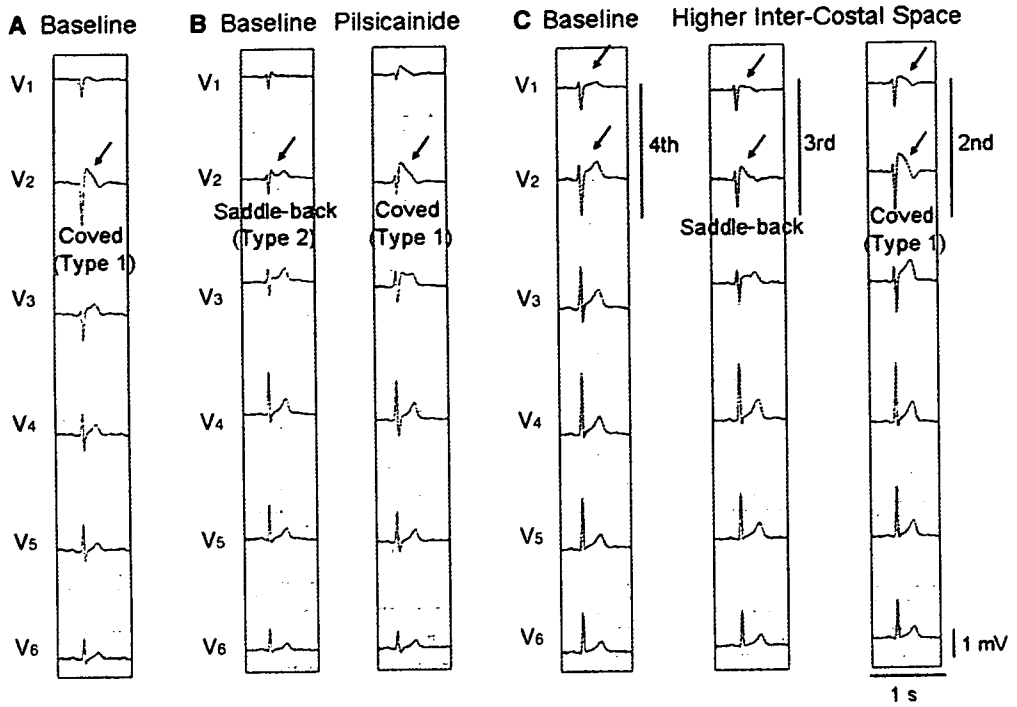

Fig 1. (A) Spontaneous type 1 coved type ST-segment elevation (arrow). (B) Unmasking of ST-segment elevation by a class IC sodium-channel blocker, pilsicainide. Under baseline conditions, type 2 saddle-back type ST-segment elevation is recorded in lead V_2 (Left, arrow). Pilsicainide injection (30 mg) unmasks the type 1 coved type ST-segment elevation in lead V_2 (Right, arrow). (C) Unmasking of the type 1 electrocardiogram (ECG) by recording the right precordial (V_{1-2}) leads at the 3rd and 2nd intercostal spaces. No significant ST-segment elevation is observed in leads V_1 and V_2 of the standard 12-lead ECG (4th intercostal space) (Left, arrow), whereas saddle-back type (Middle, arrow) and type 1 coved type (Right, arrow) ST-segment elevation are unmasked in leads V_1 and V_2 recorded from the 3rd and 2nd intercostal spaces, respectively.

These functional effects include: (1) lack of expression of the sodium channel; (2) a shift in the voltage-dependence and time-dependence of I_{Na} activation, inactivation or reactivation; (3) entry of the sodium channel into an intermediate state of inactivation from which it recovers more slowly; (4) accelerated inactivation of the sodium channel; and (5) a trafficking defect. Some common *SCN5A* polymorphisms are reported to modulate the functional consequences of primary *SCN5A* mutations. Baroudi et al first suggested that the interaction of *SCN5A* polymorphisms and *SCN5A* mutations may affect the consequence of the functional effects. They reported that a common polymorphism (R1232W) of *SCN5A* affected protein trafficking when it was co-expressed with a T1620M mutation, although the T1620M mutation alone produced only gating abnormalities in the I_{Na}.[21] On the other hand, another common polymorphism (H558R) of *SCN5A* was reported by Ye et al to rescue normal trafficking and normal I_{Na} for the M1766L mutant protein.[22] These effects of common *SCN5A* polymorphisms on modifying the functional consequence of *SCN5A* mutations may make the clinical phenotype more complex.

Cellular Mechanism of Brugada Phenotype

The I_{to}-mediated phase 1 notch of the action potential (AP) has been reported to be larger in the epicardium than in the endocardium in many species, including humans.[23] Because the maintenance of the AP dome is determined by the fine balance of currents active at the end of phase 1 of the AP (principally I_{to} and $I_{Ca\text{-}L}$), any interventions that cause a net outward shift in the current active at the end of phase 1 can increase the magnitude of the AP notch, leading to loss of the AP dome (all-or-none repolarization) in the epicardium, but not in the endocardium, contributing to a significant voltage gradient across the ventricular wall during ventricular activation.[23] The heterogeneous loss of the AP dome in the epicardium has been shown to produce premature beats via a mechanism of phase 2 reentry in experimental studies using isolated sheets of canine right ventricle.[24] Therefore, these mechanism of all-or-none repolarization in the epicardial cells and phase 2 reentry-induced premature beat between the adjacent epicardial cells were expected to be responsible for the clinical phenotype in BS.

In the late 1990s, Antzelevitch's group developed an experimental model of BS using arterially perfused canine right ventricular (RV) wedge preparations, in which transmembrane APs and pseudo-ECGs were simultaneously recorded. These experimental studies have provided significant insights of the cellular mechanism of the Brugada phenotype, ST-segment elevation and subsequent VF.[25,26] The I_{to}-mediated AP notch and the loss of the AP dome in the epicardial cells, but not in the endocardial cells, of the right ventricle gives rise to a transmural voltage gradient, producing ST-segment elevation in the ECG in the wedge preparations. Fig 2 shows transmembrane APs simultaneously recorded from 2 epicardial (Epi) and 1 endocardial sites, together with a transmural ECG in a Brugada model using the RV wedge preparation. Under control conditions, a small J wave coincides with the small notch observed in the epicardial cells, but not in the endocardial cells (Fig 2A). Combined administration of terfenadine ($I_{Ca\text{-}L}$ block) and pilsicainide (I_{Na} block) produces a loss of the AP dome in

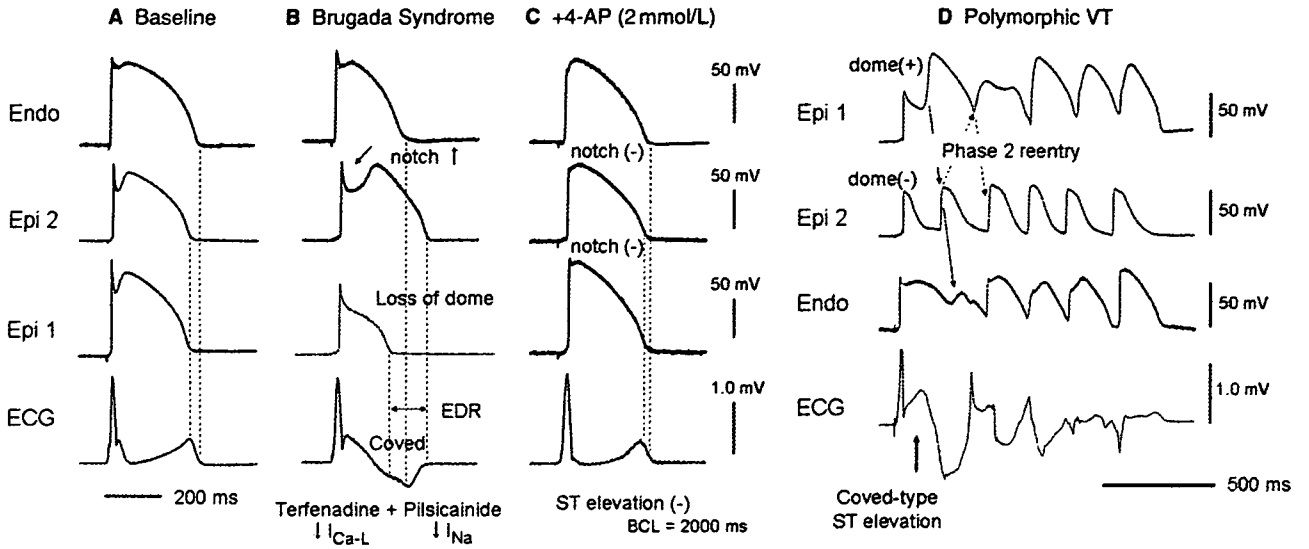

Fig 2. Type 1 coved type ST-segment elevation and non-sustained polymorphic ventricular tachycardia (VT) via phase 2 reentry induced in a Brugada model using an arterially perfused canine right ventricular wedge preparation. Shown are transmembrane action potentials (APs) simultaneously recorded from 2 epicardial sites (Epi 1 and Epi 2) and 1 endocardial site (Endo) together with a transmural ECG (basic cycle length (BCL)=2,000 ms). (A) Under baseline conditions, phase 1 AP notch in Epi, but not in Endo, is associated with a J wave in the ECG. (B) Combined administration of terfenadine (5 μmol/L) and pilsicainide (5 μmol/L) produces a loss of AP dome in Epi 1, but not in Epi 2, resulting in a marked epicardial dispersion of repolarization (EDR), and a coved-type ST segment elevation and a negative T wave in the ECG. (C) 4-aminopyridine (4-AP), a selective blocker of the transient outward current (I_{to}) (2 mmol/L), restores the AP dome, decreases the phase 1 AP notch, and normalizes the ST-segment elevation. (D) In the setting of heterogeneous loss of the AP dome (coexistence of loss of dome regions and restored dome regions) in the epicardium and a remarkable coved type ST-segment elevation in the ECG with combined administration with terfenadine and pilsicainide, electrotonic propagation from the site where the dome is restored (Epi 1) to the site where it is lost (Epi 2) results in development of a premature beat induced by phase 2 reentry, triggering spontaneous polymorphic VT (Modified from *Nat Clin Pract Cardiovasc Med* 2005; **2:** 408–414 with permission).

Epi 1, but not in Epi 2, resulting in a marked epicardial dispersion of repolarization (EDR), and a coved-type ST segment elevation and negative T wave in the ECG (Fig 2B). A selective I_{to} blocker, 4-aminopyridine, restores the AP dome, decreases the phase 1 AP notch, and normalizes the ST-segment elevation (Fig 2C). Fig 2D shows non-sustained polymorphic ventricular tachycardia (VT) via phase 2 reentry induced in a Brugada model using the wedge preparation. In the setting of remarkable coved type ST-segment elevation with combined administration of terfenadine and pilsicainide, heterogeneous loss of the AP dome (coexistence of loss of dome regions and restored dome regions) in the epicardium creates a marked EDR, giving rise to premature beats caused by phase 2 reentry, which precipitates non-sustained polymorphic VT.

Optical Mapping Study

The AP data in the Brugada model using arterially perfused canine RV wedge preparations strongly supported the hypothesis that episodes of VF in BS are triggered by premature beats between the adjacent epicardial cells via the mechanism of phase 2 reentry. However, the precise mechanism of the initial premature beats and the maintenance of non-sustained polymorphic VT or VF remain unsolved, because the number of AP recording sites available for floating microelectrodes is small in the wedge preparations. To overcome this limitation, we recently developed high-resolution (256×256) optical mapping techniques that allowed us to record transmembrane APs from 256 sites simultaneously at the epicardial or endocardial surface of the wedge preparations (Figs 3–5)[8,27] Fig 3 shows the mechanism of phase 2 reentry-induced premature beats (P2R-extrasystoles) under Brugada-ECG conditions. A steep repolarization gradient between the loss of dome region and the restored dome region in the epicardium, but not in the endocardium, develops the initial P2R-extrasystole. We then recorded spontaneous episodes of P2R-extrasystoles and subsequent non-sustained polymorphic VT or VF under these conditions, and analyzed the epicardial AP duration (APD) and conduction velocity (Figs 4,5). Once again, most of the P2R-extrasystoles originated from the area showing the steepest (maximum) gradient of repolarization (GR_{max}) between the loss of dome site and the restored dome site in the epicardium (Figs 4C,5C, arrows), leading to non-sustained polymorphic VT or VF. These data also indicate that a steep repolarization gradient between the loss of dome region and the restored dome region in the epicardium is essential to produce the P2R-extrasystoles that precipitate polymorphic VT or VF. On the other hand, the epicardial GR_{max} does not differ between episodes of polymorphic VT and those of VF. Figs 4D,E and 5D,E show the mechanism underlying the difference between polymorphic VT and VF. Just before inducing the episodes of polymorphic VT or VF, the epicardial depolarization map paced from the endocardium at the basic cycle length of 2,000 ms shows a remarkable conduction delay in the episode of VF (Fig 5D) compared with that of polymorphic VT (Fig 4D). The conduction parameters, such as QRS duration and interval between the stimulus and the earliest epicardial activation, are significantly longer in the episodes of VF than in those of polymorphic VT. Figs 4A,B

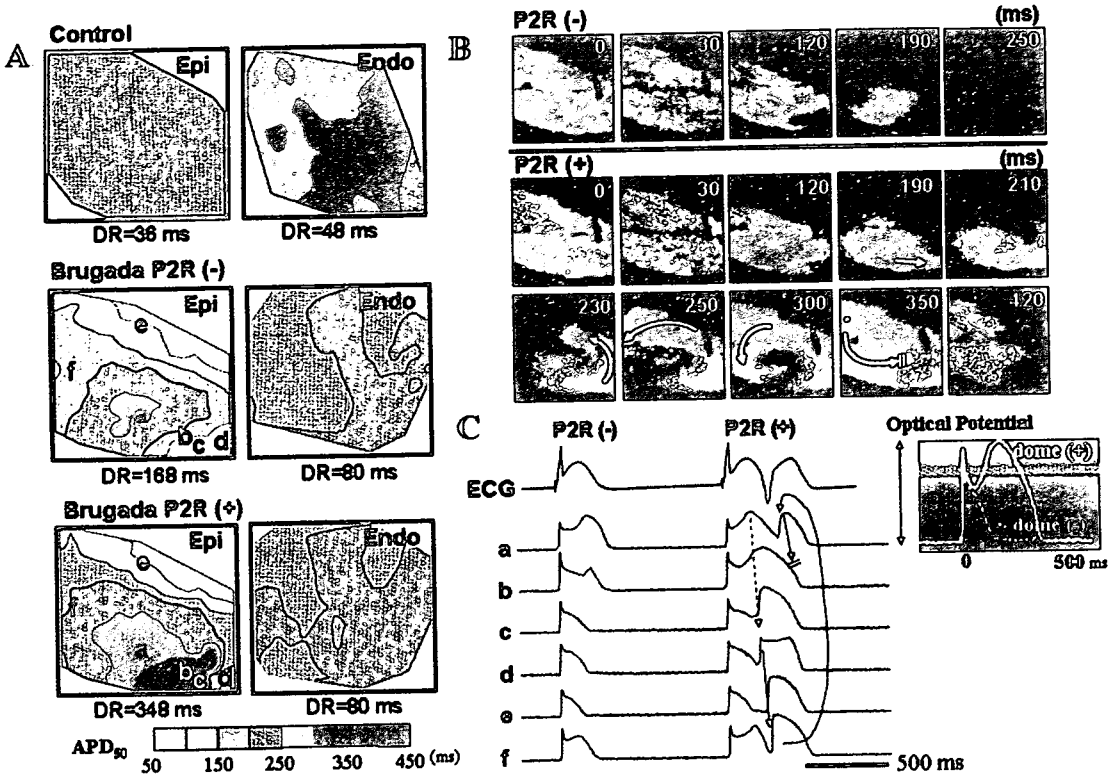

Fig 3. Mechanism of the phase 2 reentry-induced premature beats (P2R-extrasystoles) under the condition of Brugada-ECG in a model using a wedge preparation combined with high-resolution (256×256) optical mapping techniques. (A) Representative action potential duration measured at 50% (APD_{50}) contour map on the right ventricular epicardium (Epi) and endocardium (Endo) in the control, in the ST-segment elevation (Brugada-ECG) without phase 2 reentrant extrasystoles (P2R (–)) and in the Brugada-ECG just before P2R extrasystoles (P2R (+)). (B) Snapshots of an optical isopotential movie on the Epi surface during P2R(–) and P2R(+) in the Brugada-ECG. (C) Optical action potentials (APs) at each site (a–f) on the Epi surface and transmural ECG. Under the Brugada-ECG, the AP morphology in Epi, but not Endo, changes to heterogeneous because of the combination of abbreviated (loss-of-dome; site d,e) and prolonged (restore-of-dome; site a,b) APs, resulting in increasing dispersion of repolarization (DR) in Epi (168 ms) rather than in Endo (80 ms). Further prolongation of the AP in the Epi area (site b) is closely adjacent to the loss-of-dome APs (site d), thus producing a repolarization mismatch within a small area (DR = 348 ms) and developing a P2R-extrasystole at the loss-of-dome site (site d). Thus, a steep repolarization gradient in Epi, but not in Endo, develops the initial P2R-extrasystole in the Brugada-ECG (Modified from *J Am Coll Cardiol* 2006; **47:** 2074–2085 with permission).

represents a phase map and the optical APs during the P2R-induced polymorphic VT, showing that reentry is initiated from the epicardial GR_{max} area and rotates mainly in the epicardium without wave-break. In contrast, Figs 5A,B represents these during P2R-induced VF, showing that the development of the initial P2R is similar to that of polymorphic VT, but that the first P2R-wave is broken up into multiple wavelets, resulting in degeneration of VT into VF. The phase singularity points during the first P2R-wave almost coincide with the sites of delayed conduction (Fig 5D). Wave-break during the first P2R-extrasystole produces multiple wavelets in the episodes of VF, whereas no wave-break or wave-break followed by wave collision and termination occurs in the episodes of polymorphic VT. Figs 4E and 5E are histograms of the epicardial APD measured at 50% (APD_{50}) during the first P2R-wave. There is a large variety of APD_{50} in the epicardium during the first P2R-wave in the episodes of VF, whereas only slight variety in the APD_{50} is observed in the episodes of polymorphic VT. These data suggest that both conduction delay and dispersion of repolarization play significant roles in the perpetuation of VF episodes.

Late Onset of Clinical Manifestation

Because BS is a primary electrical disease, and at least one-third of the patients have mutations in ion channel genes (*SCN5A*, *CACNA1C*, *CACNB2*), clinical manifestation during childhood would be expected. However, BS usually manifests in middle age, at 40–50 years of age? Frustaci et al recently reported a significant myocytes apotosis in both the right and left ventricular myocardium in a histological study of BS patients with *SCN5A* mutations, and suggested that abnormal function of the sodium channels may lead to a sufficient degree of cellular damage, attributing to the arrhythmic event?[28] We recently analyzed several ECG parameters recorded during long-term follow-up of BS patients with and without the *SCN5A* mutation?[29] In both patient groups, the depolarization parameters, including P wave, QRS, S wave duration and PQ interval, increased with age, especially in patients with the *SCN5A* mutation. Taken together with the experimental data?[27] the findings suggest that depolarization abnormalities (conduction slowing) are required for the maintenance of VF in BS, although the initiating premature beats are caused by a phase 2 reentry mechanism.

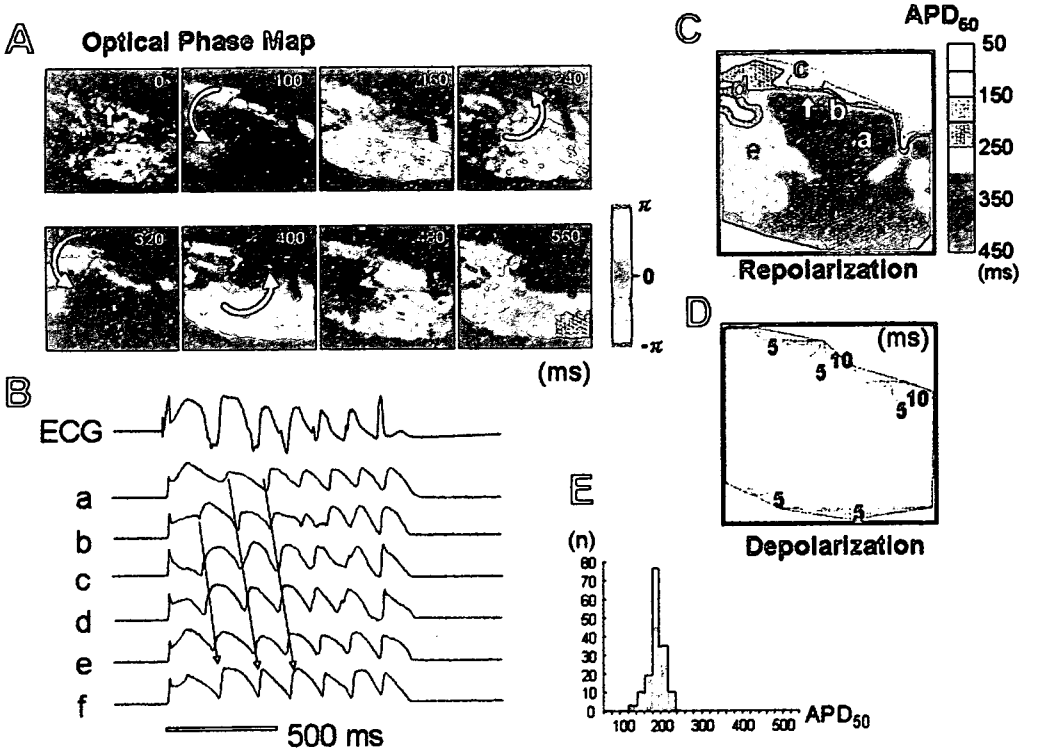

Fig4. Mechanism underlying non-sustained polymorphic ventricular tachycardia (VT) in a Brugada model using a wedge preparation combined with high-resolution (256×256) optical mapping techniques. (A) Representative snapshots from a phase movie during polymorphic VT originating from epicardial (Epi) phase 2 reentry (P2R). (B) Optical action potentials at each site (a–f), together with a transmural ECG. (C, D) Repolarization and depolarization maps on the Epi surface in the condition of Brugada-ECG just before polymorphic VT. (E) Epi action potential duration at 50% repolarization (APD_{50}) histogram during the first P2R-wave. Reentry is initiated from the steepest (maximum) repolarization gradient site in Epi (arrow in A and C) and rotates mainly in Epi without wave-break. The Epi depolarization map paced from Endo shows no conduction delay (D). There is a little variety of APD in Epi during the first P2R-wave (E). Open circles mark phase singularity points (Modified from *J Am Coll Cardiol* 2006; **47:** 2074–2085 with permission).

Male Predominance

Because all mutations so far identified in *SCN5A* display an autosomal dominant mode of transmission in BS, males and females would be expected to inherit the defective gene equally. However, an apparent male predominance is observed in patients with BS[15] Di Diego et al suggested the cellular basis for male predominance in BS while using arterially-perfused canine RV wedge preparations.[30] They reported that the I_{to}-mediated phase 1 AP notch in the RV epicardium was larger in male dogs than in female dogs was responsible for the male predominance in the Brugada phenotype. On the other hand, the male hormone, testosterone, has been reported to increase the outward potassium currents (the rapidly [I_{Kr}][31,32] and the slowly [I_{Ks}][33] activating component of I_K, and the inward rectifier potassium current [I_{K1}][32]) or decrease the inward currents ($I_{Ca\text{-}L}$).[33] Therefore, testosterone would be expected to accentuate the Brugada phenotype. Clinically, Matsuo et al report 2 cases of asymptomatic BS in which typical coved ST-segment elevation disappeared following orchiectomy as therapy for prostate cancer,[34] supporting the expectation for testosterone. Moreover, testosterone is also known to decrease visceral fat,[35] and patients with BS are thinner than the normal population.[36] On the basis of these clinical and experimental findings, we directly measured the testosterone level in male patients with BS and compared them with age-matched normal males.[37] The testosterone level was significantly higher and body mass index (BMI) significantly lower in the Brugada males than in the controls after adjusting for several confounding variables influencing testosterone level or BMI (eg, age, exercise, stress, smoking, and medication). Interestingly, testosterone level was inversely correlated with BMI in both Brugada and control males even after adjusting for confounding variables, suggesting that Brugada males have a higher testosterone level associated with lower visceral fat (Fig 6). Moreover, conditional logistic regression model analysis showed that both higher testosterone level and lower BMI independently increase the risk of BS. These data suggest that the male predominance in the Brugada phenotype is at least in part related to testosterone, which is present only in males.

Higher Incidence in Asian Population

The incidence of BS is higher in Asian countries, including Thailand and Japan, than in Western countries.[11,12,38] It has been reported that common polymorphisms might modulate the activity of the primary disease-causing mutation or influence susceptibility to arrhythmia, even in the general population.[39] The common polymorphisms may attribute to ethnic differences in the clinical phenotype in inherited cardiac arrhythmias, including BS, because some common polymorphisms are ethnically dependent. Pfeufer et al reported that polymorphisms in the *SCN5A* promoter were associated with a widening of QRS duration in a cen-

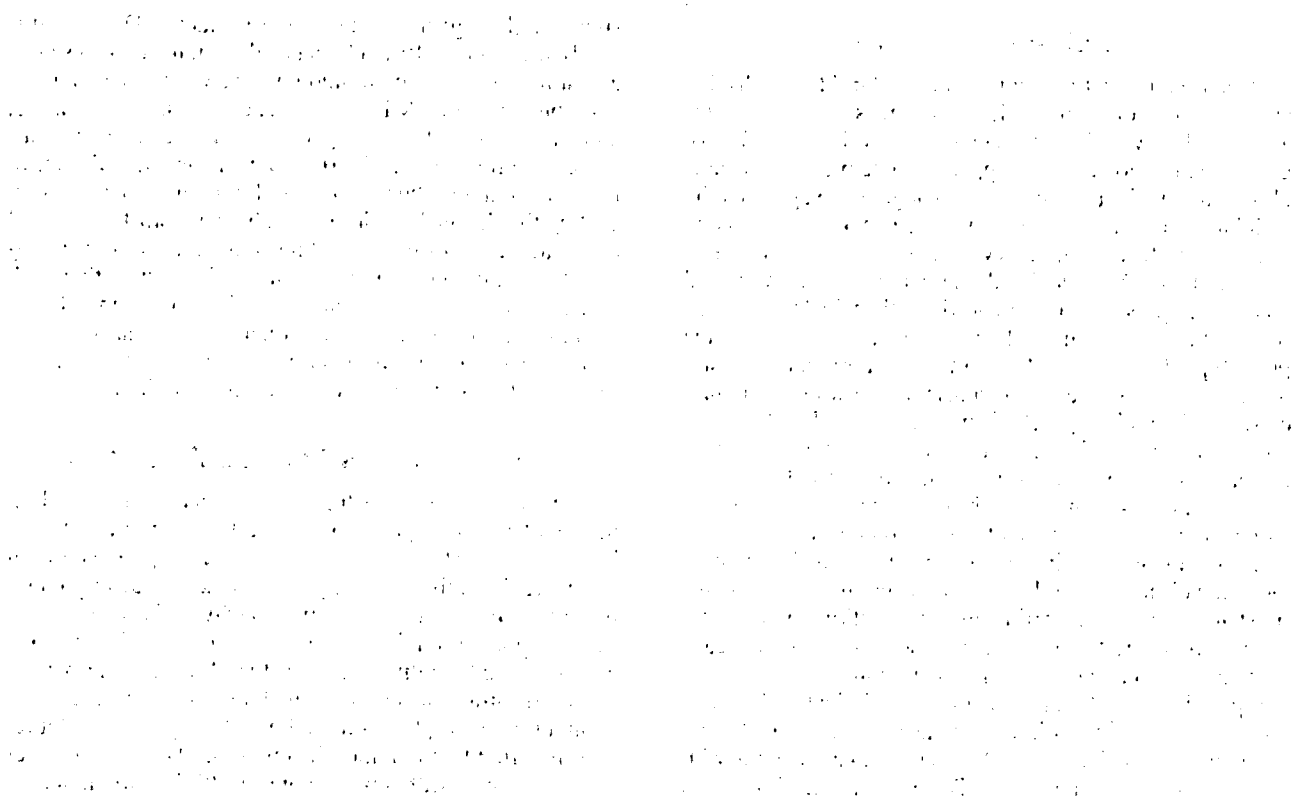

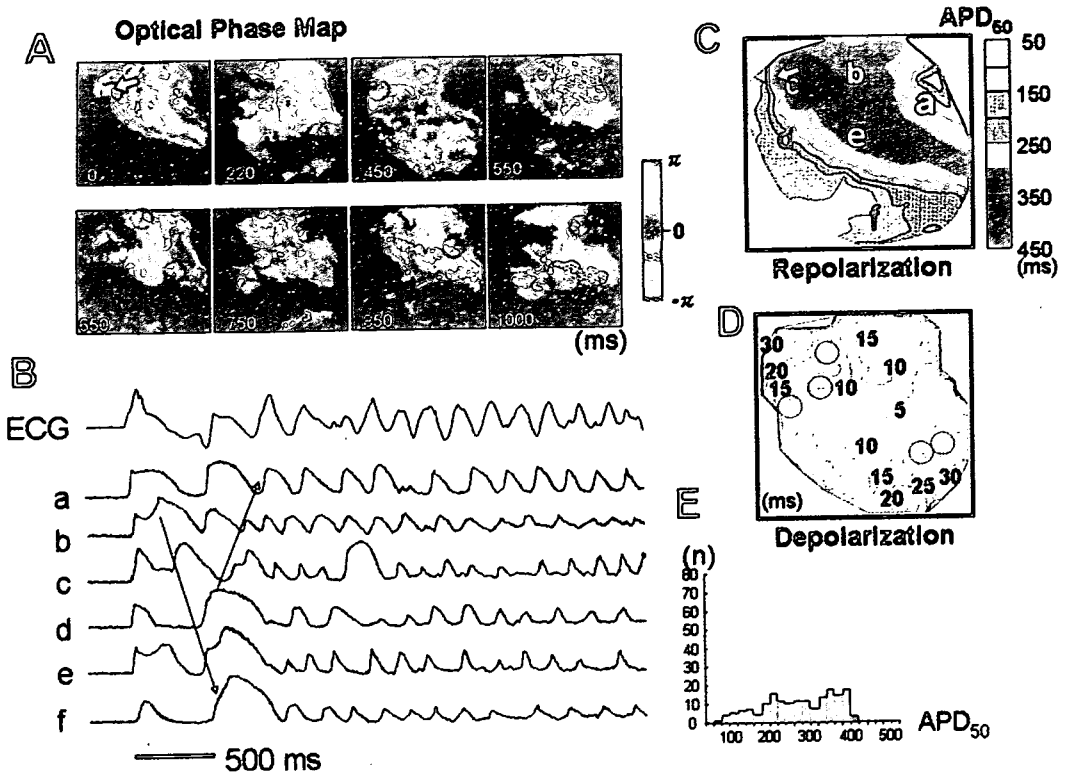

Fig5. Mechanism underlying ventricular fibrillation (VF) in a Brugada model using a wedge preparation combined with high-resolution (256×256) optical mapping techniques. (A) Representative snapshots from a phase movie during VF originating from the epicardial (Epi) phase 2 reentry (P2R). (B) Optical action potentials at each site (a–f), together with a transmural ECG. (C, D) Repolarization and depolarization maps on the Epi surface in the condition of Brugada-ECG just before VF. (E) Epi action potential duration at 50% repolarization (APD_{50}) histogram during the first P2R-wave. The area of maximum gradient of repolarization in Epi (arrow in A and C) develops the P2R. The first P2R-wave is broken up into multiple wavelets (A, 220 ms), resulting in degeneration of ventricular tachycardia into VF. The Epi depolarization map paced from the endocardium shows a remarkable conduction delay in the episode of VF (D). The phase singularity points during the first P2R-wave (open circle in D) almost coincide with the Epi sites of delayed conduction. There is a large variety of APD in Epi during the first P2R-wave (E). Thus, P2R-extrasystoles degenerate into VF with further depolarization and repolarization disturbances. Open circles mark phase singularity points (Modified from *J Am Coll Cardiol* 2006; **47:** 2074–2085 with permission).

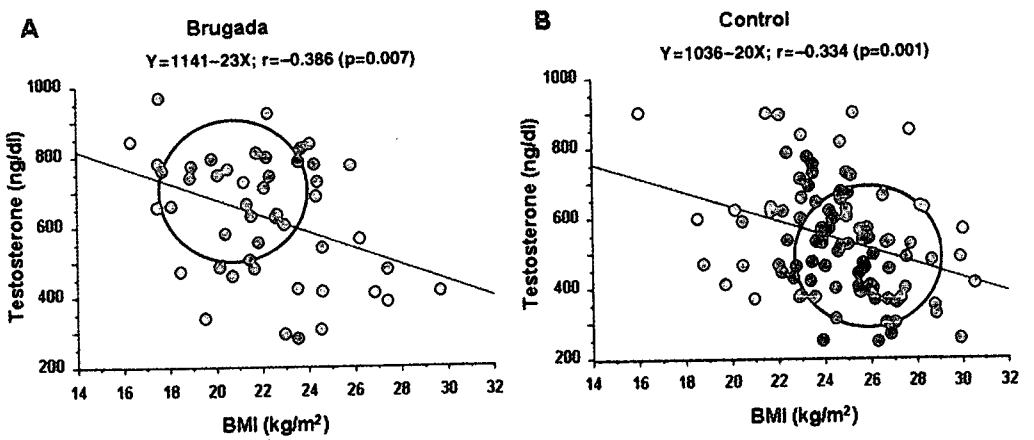

Fig6. Correlation between testosterone level and body mass index (BMI) in Brugada syndrome males and age-matched control males. Testosterone level inversely correlated withe BMI in both groups (*J Cardiovasc Electrophysiol* 2007 (in press). with permission).

tral European general population.[40] We recently identified a haplotype variant consisting of 6 individual DNA polymorphisms in near-complete linkage disequilibrium within the proximal promoter region of *SCN5A* in Asians only (an allele frequency of 22%), not in Caucasian or African-Americans (Fig 7).[41] Luciferase reporter activity of this variant haplotype, designated Haplotype B, in cardiomyocytes is reduced 62% compared with the wild-type, designated Haplotype A. To test the hypothesis that this *SCN5A* promoter polymorphism may modulate variability in cardiac